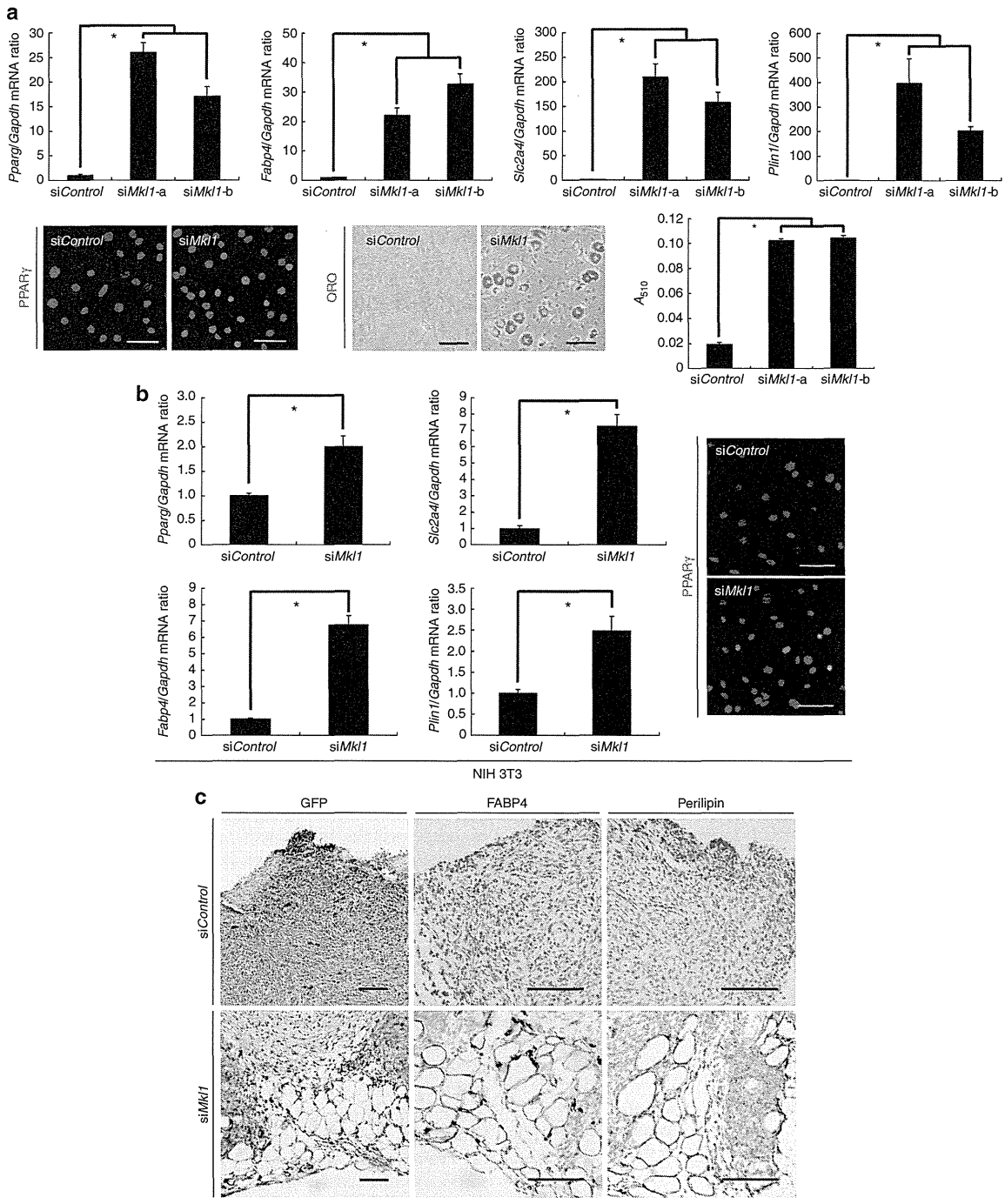


**Figure 4 | Loss of MKL1 is sufficient to drive adipocyte differentiation *in vitro* and *in vivo*.** (**a**) DFAT cells were transiently transfected with MKL1 (si*Mkl1*-a or -b) or control (si*Control*) siRNAs for 48 h and then cultured in growth medium without an adipogenic cocktail for 96 h, after which the relative abundance of *Pparg*, *Fabp4*, *Slc2a4* and *Plin1* mRNAs was determined (upper panels). The cells were also subjected to immunofluorescence analysis of PPARγ expression (bottom left panel). Nuclei were stained with Hoechst 33342. Scale bars, 100 μm. They were also stained with oil red O (bottom centre panel; Scale bars, 100 μm), and the $A_{510}$ of dye extracted from the stained cells was determined (bottom right panel). (**b**) NIH 3T3 fibroblasts were transiently transfected with MKL1 (si*Mkl1*-a) or control siRNAs for 48 h and then cultured in growth medium without an adipogenic cocktail for 96 h, after which the relative abundance of *Pparg*, *Fabp4*, *Slc2a4*, and *Plin1* mRNAs was determined (left panels). The cells were also subjected to immunofluorescence analysis of PPARγ expression (right panel). Nuclei were stained with Hoechst 33342. Scale bars, 100 μm. (**c**) DFAT cells were transiently transfected with MKL1 (si*Mkl1*-a) or control siRNAs for 48 h and then injected subcutaneously into mice. Serial sections of the injection site were subjected to immunohistochemical staining of GFP (to identify injected cells) as well as of FABP4 and perilipin (markers of terminal adipogenic differentiation) at 2 weeks after injection. The sections were counterstained with hematoxylin. Data are representative of five mice per group. Scale bars, 100 μm. All quantitative data are means ± s.d. ($n = 3$ experiments). *$P < 0.05$, Student's *t*-test.

To investigate the function of MKL1 in adipocyte differentiation *in vivo*, we transfected DFAT cells (which are derived from green fluorescent protein (GFP) transgenic mice)[12] with MKL1 siRNA for 48 h (resulting in a significant decrease in *Mkl1* expression but no change in *Pparg* expression at this time (Supplementary Fig. 5d)) and then injected the cells subcutaneously into mice. At 2 weeks after injection, many fully differentiated adipocytes were observed at the injection site in the animals that received cells transfected with MKL1 siRNA but not in those that received cells transfected with a control siRNA (Fig. 4c). The transplanted MKL1-depleted cells were thus strongly positive for markers of terminal adipogenic differentiation (FABP4 and perilipin) as well as for GFP (Fig. 4c). Together, these data revealed that MKL1 functions as a gatekeeper that controls adipocyte differentiation both *in vitro* and *in vivo*. It was previously reported that the postpartum mammary glands of Mkl1 knockout female mouse show premature involution and markedly increased white adipose tissue[34]. This phenotype of Mkl1 knockout mouse is concordant with our finding that loss of Mkl1 promotes adipocyte differentiation programme.

We also performed microarray analysis to examine the gene expression profile of cells treated with ROCK inhibitor (Y-27632) or depleted MKL1 expression by siRNA (siMkl1) and functional classification of highly expressed genes (>2-fold). The gene ontology (GO) analysis revealed the most significant biological function was 'fat cell differentiation' (GO:0045444) in both ROCK inhibition and MKL1 knockdown (Table 1). Furthermore, hierarchical clustering of all samples for 133 fat cell differentiation-associated genes demonstrated an extremely high similarity of the gene expression pattern between Y-27632 sample and siMkl1 sample (Supplementary Fig. 6a), suggesting that either ROCK inhibition or MKL1 knockdown alone predominantly induces the expression of adipocyte differentiation-associated genes in global gene expression level. Furthermore, we extracted the expression patterns of a large number of well-documented serum response factor (SRF)-MKL1 target genes[26] from those microarray data. The relative expression of these SRF-MKL1 target genes tends to decrease on ROCK inhibition and MKL1 knockdown (Supplementary Fig. 6b), suggesting that either ROCK inhibition or MKL1 knockdown in common suppresses the expression of genes downstream of MKL1.

**Table 1 | Gene ontology classifications for the highly expressed genes in ROCK inhibitor or MKL1 knockdown.**

| Gene Ontology class (Biological process with GO ID) | No. of genes in class | B-H *P*-value |
|---|---|---|
| *Y-27632>DMSO (160 genes)* | | |
| GO:0045444—fat cell differentiation | 14 | 1.57E-10 |
| GO:0050873—brown fat cell differentiation | 10 | 1.31E-08 |
| GO:0050896—response to stimulus | 58 | 4.69E-06 |
| GO:0006629—lipid metabolic process | 26 | 7.94E-05 |
| GO:0002526—acute inflammatory response | 10 | 8.33E-05 |
| *siMkl1>siControl (213 genes)* | | |
| GO:0045444—fat cell differentiation | 19 | 7.26E-16 |
| GO:0050873—brown fat cell differentiation | 15 | 8.58E-16 |
| GO:0006629—lipid metabolic process | 33 | 6.41E-06 |
| GO:0044255—cellular lipid metabolic process | 27 | 5.40E-06 |
| GO:0002526—response to hormone stimulus | 16 | 7.75E-06 |

GO analysis were performed individually on the highly expressed genes (>2-fold) in Y-27632 sample (160 genes) or in siMkl1 sample (213 genes). All functional categories demonstrated enhanced statistical representation.

**PPARγ induces *Mkl1* downregulation during adipogenesis.** We noticed that treatment with Y-27632, which elicited remodelling of the actin cytoskeleton, not only prevented nuclear translocation of MKL1 but also induced a significant decrease in the amount of *Mkl1* mRNA in DFAT cells and 3T3-L1 preadipocytes (Supplementary Fig. 3i). Moreover, we found that *Mkl1* expression correlated inversely with *Pparg* expression during adipocytic differentiation (Fig. 5a). To test whether PPARγ contributes to *Mkl1* downregulation during adipogenesis, we investigated the effect of PPARγ knockdown on *Mkl1* expression. We established DFAT cells stably depleted of PPARγ as a result of retrovirus-mediated expression of a specific short hairpin RNA (shRNA) (Fig. 5b). Although control cells expressing a luciferase shRNA manifested a significant decrease in the abundance of *Mkl1* mRNA after exposure to inducers of adipocytic differentiation, cells expressing the PPARγ shRNA did not (Fig. 5b). To clarify further the influence of PPARγ on *Mkl1* expression, we generated DFAT cells that stably overexpress PPARγ (Fig. 5c). Overexpression of PPARγ resulted in a significant decrease in the amount of *Mkl1* mRNA (Fig. 5c), indicating that PPARγ indeed suppresses the expression of *Mkl1*, resulting in the continuous activation of PPARγ required for the completion of adipocyte differentiation.

## Discussion

On the basis of our observations, we propose a model for the control of adipocyte differentiation in which regulation of MKL1 by disruption of actin stress fibres triggers the differentiation programme (Fig. 5d). Exposure of preadipocytes to an adipogenic cocktail results in the rapid disruption of actin stress fibres as a consequence of downregulation of RhoA-ROCK signalling. The resulting increase in the amount of G-actin leads to the binding of G-actin to MKL1 and to inhibition of the nuclear translocation and transcriptional regulatory activity of the latter protein. Transcription of the *Pparg* gene is thereby activated, and the encoded protein then mediates not only upregulation of the expression of genes (such as *Fabp4*, *Plin* and *Slc2a4*) associated with the adipocyte phenotype but also downregulation of *Mkl1* expression to allow completion of adipogenesis.

Several preadipocyte cell lines undergo differentiation on treatment with a standard adipogenic cocktail consisting of IBMX, dexamethasone and insulin[35]. Both IBMX and dexamethasone trigger the activation of protein kinase A by increasing the intracellular concentration of cAMP, thereby promoting adipocyte differentiation[36]. The major role of protein kinase A in adipogenesis has been thought to lie in downregulation of RhoA and ROCK activity[37]. In the present study, we found that Rho activity is rapidly reduced after treatment of DFAT cells with the adipogenic cocktail, and the downregulation of RhoA-ROCK signalling then promotes adipocyte differentiation via modulation of remodelling of the actin cytoskeleton. In addition, we found that treatment with LatA alone or Y-27632 alone, by inducing remodelling of the actin cytoskeleton, is sufficient to trigger adipocyte differentiation in the absence of an adipogenic cocktail. Our findings, combined with previous observations, thus suggest that a standard adipogenic cocktail directly elicits reorganization of the actin cytoskeleton through downregulation of RhoA-ROCK signalling, and that the disruption of actin stress fibres then acts as a trigger for the adipocytic differentiation of preadipocytes *in vitro*.

In differentiated adipocytes, cortical F-actin has an important regulatory role in the insulin-stimulated translocation of the glucose transporter GLUT4 (encoded by *Slc2a4*) from intracellular storage sites to the plasma membrane[10], with the formation of cortical F-actin thus likely being a key event in adipogenesis.

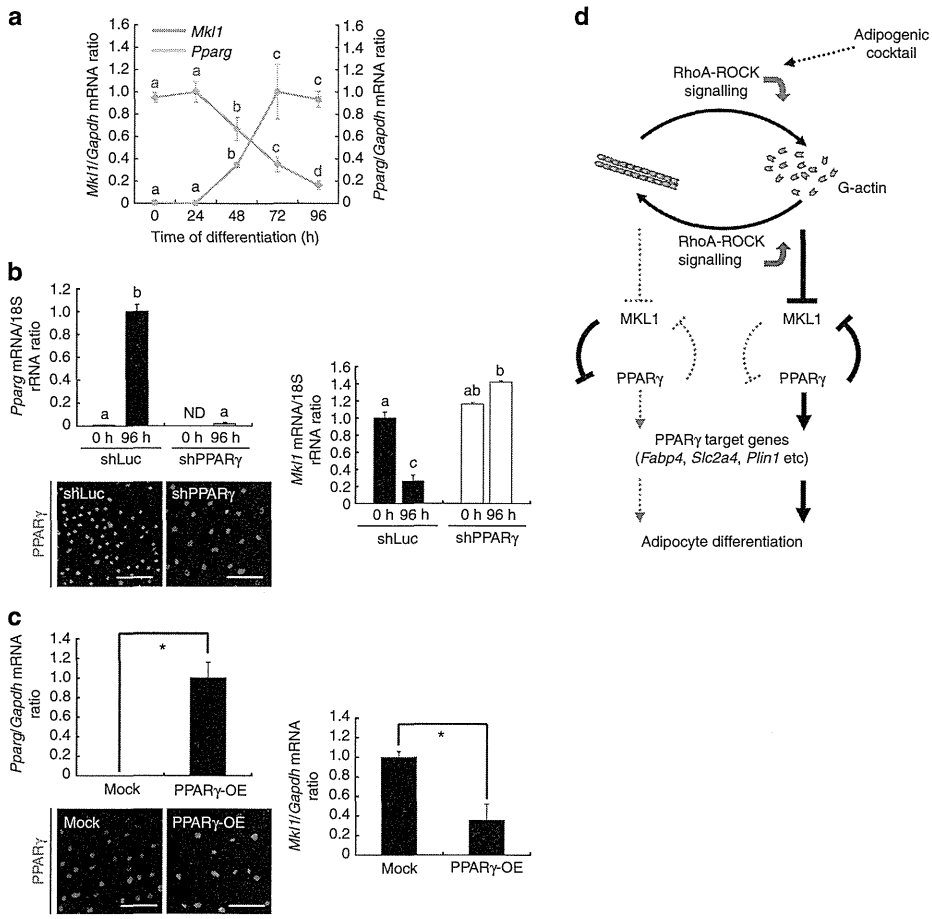


**Figure 5 | PPARγ contributes to *Mkl1* downregulation during adipocyte differentiation.** (**a**) The relative abundance of *Mkl1* and *Pparg* mRNAs at the indicated times after exposure of DFAT cells to inducers of adipocytic differentiation was also determined. (**a–c**) $P<0.05$, (**a–d**) $P<0.05$, Tukey's honest significant difference test. (**b**) DFAT cells stably expressing PPARγ (shPPARγ) or luciferase (shLuc, control) shRNAs were exposed to inducers of adipogenesis for 0 or 96 h and then assayed for the relative abundance of *Pparg* and *Mkl1* mRNAs. The cells were also subjected to immunofluorescence analysis of PPARγ after 96 h. Nuclei were stained with Hoechst 33342. Scale bars, 100 μm. ND, not detected. (**c**) DFAT cells stably overexpressing PPARγ (PPARγ-OE) or infected with the corresponding empty vector (Mock) were assayed for the relative abundance of *Pparg* and *Mkl1* mRNAs. *$P<0.05$, Student's *t*-test. They were also subjected to immunofluorescence analysis of PPARγ expression. Nuclei were stained with Hoechst 33342. Scale bars, 100 μm. All quantitative data are means ± s.d. ($n=3$ experiments). (**d**) Model for the regulation of adipocyte differentiation. Regulation of MKL1 by disruption of actin stress fibres drives adipocyte differentiation.

In the present study, F-actin stress fibres were depolymerized to G-actin within 24 h after the induction of adipocyte differentiation, and the actin cytoskeleton was subsequently reorganized to form cortical F-actin structures within 48 h. The abundance of transcripts for MKL1, which binds to G-actin, began to decline within 48 h after induction of adipocyte differentiation, and this downregulation of *Mkl1* was controlled by PPARγ. We also found that cells depleted of PPARγ maintained a high level of *Mkl1* expression even after induction of adipocyte differentiation, and that these cells manifested disruption of actin stress fibres at 24 h but not the formation of cortical F-actin structures even at 96 h (Supplementary Fig. 4e). Together, these observations suggest that the downregulation of *Mkl1* expression not only contributes to the continued activation of PPARγ but also promotes the organization of adipocyte-specific cortical F-actin structures as a result of the release of G-actin from MKL1–G-actin complexes.

Our findings provide new insight into the regulatory mechanism of adipocyte differentiation, which is shown to be triggered through regulation of MKL1 resulting from disruption of actin stress fibres. They also identify MKL1 as a novel gatekeeper in the regulation of adipogenesis as well as provide a basis for further studies of the relation between the dynamics of cell shape and transcription factor function during cellular differentiation. Lastly, given that activating mutations of RAC protein, which belongs to the RHO family of small GTPases and orchestrates actin polymerization, were found in a wide variety of human cancers and given their marked transforming ability[38], we assume that aberrant differentiation associated with actin cytoskeleton dynamics can be a critical factor of tumorigenesis, and our works thus would potentially contribute to understanding cancer biology.

## Methods

**Cell culture.** The mouse preadipocyte cell line DFAT was established from dedifferentiated mature adipocytes of GFP transgenic mice by ceiling culture (a method to culture lipid-containing adipocytes based on their lipid buoyancy)[12]. The mouse embryonic preadipocyte cell line 3T3-L1 and the mouse embryonic fibroblast cell line NIH 3T3 were obtained from the Japanese Collection of Research Bioresources (Tokyo, Japan). DFAT, 3T3-L1, or NIH 3T3 cells were cultured under a humidified atmosphere of 5% $CO_2$ and 95% air at 37 °C on glass

coverslips (Matsunami, Osaka, Japan) placed in tissue culture dishes (Falcon 3001; BD, Bedford, MA) containing Dulbecco's modified Eagle's medium (DMEM) (Nissui Pharmaceutical, Tokyo, Japan) supplemented with 10% fetal bovine serum (FBS) (Moregate BioTech, Bulimba, Queensland, Australia). DFAT or 3T3-L1 cells were grown to semiconfluence before induction of differentiation by exposure to DMEM supplemented with FBS (1% or 10%, respectively), 0.5 mM IBMX (Wako, Osaka, Japan), 0.1 μM dexamethasone (Wako), and insulin-transferrin-selenium-X supplement (final insulin concentration of 5 μg ml$^{-1}$) (Invitrogen, Carlsbad, CA).

**Time-lapse imaging.** For time-lapse observation of actin dynamics during adipocyte differentiation, DFAT cells were infected with Cellular Lights Actin-RFP baculovirus expression vectors (Invitrogen) and then cultured in a glass-bottomed dish (Iwaki, Chiba, Japan). After the cells achieved semiconfluence, adipocyte differentiation was induced as described above and time-lapse fluorescence and differential interference contrast video microscopy was performed with the use of a microscope (Olympus LCV110) equipped with an incubation chamber. Images were acquired every 30 min with the use of a charge-coupled device camera (Retiga Exi, QImaging) equipped with a U Plan Super Apochromatic × 40, 0.95 numerical aperture objective and were analysed with MetaMorph software (Molecular Devices, Sunnyvale, CA).

**RT and real-time PCR analysis.** Total RNA was isolated from cells with the use of the Trizol reagent (Invitrogen), and portions (1 μg) of the DNase I–treated RNA were subjected to reverse transcription (RT) with the use of high-capacity RNA-to-cDNA master mix (Applied Biosystems, Foster City, CA). The probes for PPARγ (*Pparg*; GenBank accession no. NM_011146.3; Mm00440940_m1), C/EBPα (*Cebpa*; GenBank accession no. NM_007678.3; Mm00514283_s1), fatty acid-binding protein 4 (*Fabp4*; GenBank accession no. NM_024406.2; Mm00445878_m1), GLUT4 (*Slc2a4*; GenBank accession no. NM_009204.2; Mm01245502_m1), perilipin 1 (*Plin1*; GenBank accession no. NM_175640.2; Mm00558672_m1) and MKL1 (*Mkl1*; GenBank accession no. NM_153049.2; Mm00461840_m1) genes were obtained fromTaqMan Pre-Developed Assay Reagents (Applied Biosystems). A mouse glyceraldehyde-3-phosphate dehydrogenase (*Gapdh*; GenBank accession no. NM_008084.2) TaqMan probe (4352339E, Applied Biosystems) or eukaryotic 18S rRNA (GenBank accession no. X03205.1) TaqMan probe (4319413E, Applied Biosystems) was included as an endogenous control. The RT products (2 μl) were subjected to real-time PCR analysis in a final volume of 10 μl with the use of TaqMan Fast Universal PCR master mix (Applied Biosystems) and with an ABI7500 thermocycler. Each sample was assayed in triplicate.

**Immunoblot analysis.** Cells were washed extensively with phosphate-buffered saline (PBS) and then either recovered directly with a rubber scraper in SDS sample buffer (62.5 mM Tris-HCl (pH 6.8), 10% SDS, 5% glycerol, 5% β-mercaptoethanol, 10% bromophenol blue) or subjected to extraction of nuclear and cytoplasmic fractions with the use of an NE-PER nuclear and cytoplasmic extraction reagent kit (Pierce, Rockford, IL). Samples were subjected to SDS–polyacrylamide gel electrophoresis, the separated proteins were transferred electrophoretically to a polyvinylidene difluoride membrane (Millipore, Bedford, MA), and nonspecific sites of the membrane were then blocked by incubation with Blocking One (Nacalai Tesque, Kyoto, Japan) for 1 h at room temperature. The membrane was then exposed for 24 h at 4 °C to rabbit polyclonal antibodies to PPARγ (1:500 dilution; P0744; Sigma-Aldrich, St Louis, MO), to lamin A/C (1:500 dilution; #2032; Cell Signalling Technology, Beverly, MA), or to MEK1/2 (1:500 dilution; #9122; Cell Signalling Technology); rabbit monoclonal antibodies to cofilin (1:1,000 dilution; #5175; Cell Signalling Technology); or mouse monoclonal antibodies to FLAG (1:1,000 dilution; F1804; Sigma-Aldrich), to GAPDH (1:10,000 dilution; G8795; Sigma-Aldrich), or to α-tubulin (1:10,000 dilution; T5168; Sigma-Aldrich). The membrane was washed with PBS containing 0.02% Tween 20, incubated for 1 h at room temperature with horseradish peroxidase–conjugated goat antibodies to rabbit or mouse immunoglobulin G (1:2,000 dilution; GE Healthcare, Tokyo, Japan), and washed again with PBS containing 0.02% Tween 20, after which immunoreactive proteins were visualized with the use of enhanced chemiluminescence reagents (GE Healthcare). Uncropped scans of the most important western blots were shown in Supplementary Fig. 7.

**Immunofluorescence staining.** Cells were fixed overnight at 4 °C in zinc fixative solution (0.1 M Tris-HCl (pH 7.4), calcium acetate (475 μg ml$^{-1}$), zinc acetate (5 mg ml$^{-1}$) and $ZnCl_2$ (5 mg ml$^{-1}$) in ultrapure water) containing 0.2% Triton X-100. They were then washed in Tris-buffered saline (TBS) and incubated for 1 h at room temperature with 10% normal goat or horse serum (Vector Laboratories, Burlingame, CA) and 1% bovine serum albumin (BSA) (Sigma-Aldrich) in TBS to block nonspecific binding of antibodies before staining with primary antibodies according to standard procedures. Primary antibodies included rabbit monoclonal antibodies to PPARγ (1:200 dilution; #2435; Cell Signalling Technology); rabbit polyclonal antibodies to perilipin A/B (1:1,000 dilution; P1873; Sigma-Aldrich) and to MKL1 (1:100 dilution; ab49311; Abcam, Cambridge, MA); and mouse monoclonal antibodies to β-actin (1:1,000 dilution; A5441; Sigma-Aldrich), to HA (1:500 dilution; 1583816; Roche, Mannheim, Germany), and to FLAG (1:1,000 dilution; F1804; Sigma-Aldrich). Immune complexes were detected with Alexa Fluor 488– or Alexa Fluor 594–conjugated goat antibodies to rabbit or mouse immunoglobulin G (each at 1:2,000 dilution; Molecular Probes, Eugene, OR). Antibodies were diluted in TBS containing 1% BSA. F-actin was stained with Alexa Fluor 488– or Alex Fluor 594–labelled phalloidin (Molecular Probes) at 200 U ml$^{-1}$ in TBS, and G-actin was stained with Alexa Fluor 594–labelled DNase I (Molecular Probes) at 9 μg ml$^{-1}$ in TBS. Cells were counterstained with Hoechst 33342 (Sigma-Aldrich) at 5 μg ml$^{-1}$ in TBS and were observed with a laser-scanning confocal microscope (Olympus FV-750) and a BIOREVO BZ-9000 fluorescence microscope (Keyence, Osaka, Japan).

**Lipid staining.** Lipid accumulation in adipocytes was detected by staining with oil red O (Wako). Cells were washed three times with PBS, fixed for 1 h at room temperature with 10% formalin in phosphate buffer, washed again with PBS and stained for 15 min at room temperature with a filtered solution of oil red O (0.5 g in 100 ml of isopropyl alcohol). The cells were then washed twice with distilled water for 15 min. For quantitation of lipid accumulation, dimethyl sulfoxide (DMSO) (500 μl per 35-mm dish) was added to the washed and dried cells for 1 min, after which the absorbance of the extracted dye at 510 nm was measured with a spectrophotometer (ND-1000; Nanodrop Technologies, Wilmington, DE) and was normalized by dish area.

**Pharmacological agents.** Cells were exposed to the following agents: 5 μM phalloidin oleate (Calbiochem, San Diego, CA) dissolved in DMSO, 30 μM Y-27632 (Calbiochem) dissolved in water, 0.2 μM cytochalasin D (CytD) (Sigma-Aldrich) dissolved in DMSO, 0.4 μM latrunculin A (LatA) (Calbiochem) dissolved in DMSO, 0.1 μM swinholide A (SwinA) (Calbiochem) dissolved in ethanol or 1 μM 4-hydroxytamoxifen (TAM) (Sigma-Aldrich) dissolved in ethanol.

**Rho activation assay.** Cells were lysed by incubation with a magnesium-containing buffer (25 mM HEPES-NaOH (pH 7.5), 150 mM NaCl, 1% Igepal CA-630 detergent, 10 mM $MgCl_2$, 1 mM EDTA, 2% glycerol) supplemented with 25 mM NaF, 1 mM $Na_3VO_4$, and a protease inhibitor cocktail (Nacalai Tesque). The lysates were centrifuged at 14,000 × *g* for 5 min at 4 °C, and the resulting supernatants were incubated for 45 min at 4 °C with 25 μg of a glutathione S-transferase fusion protein of the Rho-binding domain (amino acids 7–89) of rhotekin that was bound to glutathione-Sepharose beads (Millipore). The beads were washed three times with the magnesium-containing buffer and then subjected to immunoblot analysis with mouse monoclonal antibodies to RhoA, -B and -C (1:250 dilution; #05-778; Millipore). Whole-cell lysates were also subjected to immunoblot analysis with the antibodies to Rho and those to GAPDH (loading control).

**Transplantation and histological evaluation.** All animal studies were performed according to the NIH Guide for the Care and Use of Laboratory Animals. C57BL/6J mice were obtained from Oriental Yeast (Tokyo, Japan). DFAT cells ($1 \times 10^5$) collected with the use of a cell scraper were injected subcutaneously with a syringe above the sternum of 10 female mice at 8 weeks of age. After 2 weeks, cells at the injection site were retrieved, fixed in paraformaldehyde and embedded in paraffin. For immunohistochemical analysis, tissue sections were depleted of paraffin, washed with TBS, and stained with the use of a Vectastain ABC kit (Vector Laboratories). Primary antibodies included rabbit polyclonal antibodies to GFP (1:100 dilution; sc-8334; Santa Cruz Biotechnology, Santa Cruz, CA), to FABP4 (1:1,000 dilution; ab13979; Abcam) and to perilipin A/B (1:1,000 dilution; P1873; Sigma-Aldrich). The sections were counterstained with hematoxylin (Wako).

**Plasmid transfection.** The plasmids pEF-BOS-HA-RhoAV14 and pEF-BOS-HA-RhoAN19 (ref. 39) plasmids were transfected into DFAT cells for 24 h using the Fugene HD reagent (Roche).

**RNAi.** Expression of shRNAs was achieved with the retroviral expression vector pRePS (kindly provided by T. Hara), which also contains a puromycin resistance gene. The sequences of the sense oligonucleotides were 5′-GTTTGAGTTTG CTGTGAAG-3′ for PPARγ shRNA[40] and 5′-CGTACGCGGAATACTTCGA-3′ for luciferase shRNA (nonspecific control). pReps vectors transfected into Plat-E packaging cells[41] using Fugene HD (Roche). Medium was replaced once after 24 h, and viral supernatants were collected and filtered with 0.45-μm cellulose acetate filters (Iwaki) 48 h after transfection. Retroviral infection was carried out in a six-well plate for 48 h, and infected cells were then subjected to selection in the presence of puromycin (10 μg ml$^{-1}$). The sequences of siRNAs targeting cofilin1 were 5′-GAUGAACACCAGGUCCUCCUU-3′ for *Cfl1*-a, 5′-AAGAUCAAAAG CAGUUUGGGA-3′ for *Cfl1*-b, and 5′-UCACUAUUGUGGUUAGAAGUU-3′ for *Cfl1*-c, and those of siRNAs targeting MKL1 were 5′-CGAGGACUAUUUGAAA CGGAA-3′ for *Mkl1*-a and 5′-CCCACUCAGGUUCUUUCUCAA-3′ for *Mkl1*-b. The control siRNA sequence was 5′-GCGCGCUUUGUAGGAUUCG-3′. Cells

were transfected with siRNA duplexes for 48 h with the use of Lipofectamine RNAiMAX (Invitrogen).

**Retroviral gene transfer.** The coding region for mCherry cDNA was amplified from the vector containing mCherry-MKlp2 (ref. 42) by PCR with the primers 5′-CCGCTCGAGATGGTGAGCAAGGGCGAGGAGGATAACATG-3′ (XhoI_mCherry forward primer) and 5′-CGGAATTCTTCTTGTACAGCT CGTCCATGCCGCCGGTGG-3′ (mCherry_EcoRI reverse primer), and the coding region for human ER was amplified from the pMV7-MycER plasmid[43] by PCR with the primers 5′-CCGCTCGAGTCTGCTGGAGACATGAGAGCTGCCAA CCTT-3′ (XhoI_ER forward primer) and 5′-CGGAATTCTTGACCGTGGCAG GGAAACCCTCTGCCTCCCC-3′ (ER_EcoRI reverse primer), digested with XhoI and EcoRI, and ligated into the XhoI and EcoRI sites of pMXs-3 × FLAG-IP[42]. Human cDNAs for full-length MKL1 and MKL1-N100 were obtained by digestion of Addgene Plasmids (#11978, #27176)[32] with EcoRI and BamHI, and the resulting fragments were cloned into the EcoRI and BamHI sites of pMXs-3 × FLAG-mCherry-IP and/or pMXs-3 × FLAG-ER-IP. The resulting vectors were designated pMXs-3 × FLAG-mCherry-MKL1-IP, pMXs-3 × FLAG-ER-MKL1-IP, or pMXs-3 × FLAG-ER-MKL1-N100-IP, and pMXs-3 × FLAG-mCherry-IP or pMXs-3 × FLAG-ER-IP was used as a control. Mouse PPARγ cDNA (ImaGenes, Berlin, Germany) was cloned into the retroviral plasmid pMXs-puro (kindly provided by T. Kitamura). pMXs vectors were transfected into Plat-E packaging cells[44] using FugeneHD (Roche). Medium was replaced once after 24 h, and viral supernatants were collected and filtered with 0.45-μm cellulose acetate filters (Iwaki) 48 h after transfection. Retroviral infection was carried out in a six-well plate for 48 h, and infected cells were subjected to selection in the presence of puromycin (10 μg ml$^{-1}$).

**Microarray analysis.** The quality of RNA was assessed using the Agilent 2100 Bioanalyzer (Agilent Technologies, Waldbronn, Germany). The RNA samples were labelled using the GeneChip One-Cycle Target Labeling and Control Reagent pakage (Affymetrix, Santa Clara, CA) and then hybridized to the Affymetrix GeneChip mouse genome 430 2.0 array according to the manufacturer's instruction. Fluorescent images were visualized using a GeneChip Scanner 3000 (Affymetrix). Expression and raw expression data (CEL files) were summarized and normalized using the Robust Multi-array Average algorithm and the Bioconductor package affy (http://www.bioconductor.org/packages/2.0/bioc/html/affy.html). The Spotfire DecisionSite for Functional Genomics software package (TIBCO Software, Palo Alto, CA) was used for visualization of microarray data. Functional analyses were performed using DAVID Bioinformatics Resources 6.7 (http://david.abcc.ncifcrf.gov/). Functional analysis identified the biological functions that were most significant to the data set.

**Statistical analysis.** Data are presented as means ± s.d. and were analysed with Tukey's honest significant difference test or Student's *t*-test for comparisons between two or among three or more groups, respectively. A *P*-value of $<0.05$ was considered statistically significant.

## References


1. Braun, T. & Gautel, M. Transcriptional mechanisms regulating skeletal muscle differentiation, growth and homeostasis. *Nat. Rev. Mol. Cell Biol.* **12,** 349–361 (2011).
2. de Crombrugghe, B., Lefebvre, V. & Nakashima, K. Regulatory mechanisms in the pathways of cartilage and bone formation. *Curr. Opin. Cell Biol.* **13,** 721–727 (2001).
3. Farmer, S. R. Transcriptional control of adipocyte formation. *Cell Metab.* **4,** 263–273 (2006).
4. Wu, Z. *et al.* Cross-regulation of C/EBPα and PPARγ controls the transcriptional pathway of adipogenesis and insulin sensitivity. *Mol. Cell* **3,** 151–158 (1999).
5. Tontonoz, P., Hu, E. & Spiegelman, B. M. Stimulation of adipogenesis in fibroblasts by PPARγ2, a lipid-activated transcription factor. *Cell* **79,** 1147–1156 (1994).
6. Okuno, M., Arimoto, E., Nishizuka, M., Nishihara, T. & Imagawa, M. Isolation of up- or down-regulated genes in PPARγ-expressing NIH3T3 cells during differentiation into adipocytes. *FEBS Lett.* **519,** 108–112 (2002).
7. Rosen, E. D. & MacDougald, O. A. Adipocyte differentiation from the inside out. *Nat. Rev. Mol. Cell Biol.* **7,** 885–896 (2006).
8. Smas, C. M. & Sul, H. S. Control of adipocyte differentiation. *Biochem. J.* **309,** 697–710 (1995).
9. Jaffe, A. B. & Hall, A. Rho GTPases: biochemistry and biology. *Annu. Rev. Cell Dev. Biol.* **21,** 247–269 (2005).
10. Kanzaki, M. & Pessin, J. E. Insulin-stimulated GLUT4 translocation in adipocytes is dependent upon cortical actin remodeling. *J. Biol. Chem.* **276,** 42436–42444 (2001).
11. Noguchi, M. *et al.* Genetic and pharmacological inhibition of Rho-associated kinase II enhances adipogenesis. *J. Biol. Chem.* **282,** 29574–29583 (2007).
12. Nobusue, H., Endo, T. & Kano, K. Establishment of a preadipocyte cell line derived from mature adipocytes of GFP transgenic mice and formation of adipose tissue. *Cell Tissue Res.* **332,** 435–446 (2008).
13. Yagi, K., Kondo, D., Okazaki, Y. & Kano, K. A novel preadipocyte cell line established from mouse adult mature adipocytes. *Biochem. Biophys. Res. Commun.* **321,** 967–974 (2004).
14. Spiegelman, B. M. & Ginty, C. A. Fibronectin modulation of cell shape and lipogenic gene expression in 3T3-adipocytes. *Cell* **35,** 657–666 (1983).
15. McBeath, R., Pirone, D. M., Nelson, C. M., Bhadriraju, K. & Chen, C. S. Cell shape, cytoskeletal tension, and RhoA regulate stem cell lineage commitment. *Dev. Cell* **6,** 483–495 (2004).
16. Kilian, K. A., Bugarija, B., Lahn, B. T. & Mrksich, M. Geometric cues for directing the differentiation of mesenchymal stem cells. *Proc. Natl Acad. Sci. USA* **107,** 4872–4877 (2010).
17. Dupont, S. *et al.* Role of YAP/TAZ in mechanotransduction. *Nature* **474,** 179–183 (2011).
18. Cristancho, A. G. & Lazar, M. A. Forming functional fat: a growing understanding of adipocyte differentiation. *Nat. Rev. Mol. Cell Biol.* **12,** 722–734 (2011).
19. Ridley, A. J. & Hall, A. The small GTP-binding protein Rho regulates the assembly of focal adhesions and actin stress fibres in response to growth factors. *Cell* **70,** 389–399 (1992).
20. Riento, K. & Ridley, A. J. Rocks: multifunctional kinases in cell behaviour. *Nat. Rev. Mol. Cell Biol.* **4,** 446–456 (2003).
21. Hamm, J. K., El Jack, A. K., Pilch, P. F. & Farmer, S. R. Role of PPARγ in regulating adipocyte differentiation and insulin-responsive glucose uptake. *Ann. NY Acad. Sci.* **18,** 134–145 (1999).
22. Tashiro, K. *et al.* Efficient adenovirus vector-mediated PPARγ gene transfer into mouse embryoid bodies promotes adipocyte differentiation. *J. Gene Med.* **10,** 498–507 (2008).
23. Tontonoz, P. & Spiegelman, B. M. Fat and beyond: the diverse biology of PPARγ. *Annu. Rev. Biochem.* **77,** 289–312 (2008).
24. Qian, S. W. *et al.* Characterization of adipocyte differentiation from human mesenchymal stem cells in bone marrow. *BMC Dev. Biol.* **10,** 47 (2010).
25. Bamburg, J. R. Proteins of the ADF/cofilin family: essential regulators of actin dynamics. *Annu. Rev. Cell Dev. Biol.* **15,** 185–230 (1999).
26. Olson, E. N. & Nordheim, A. Linking actin dynamics and gene transcription to drive cellular motile functions. *Nat. Rev. Mol. Cell Biol.* **11,** 353–365 (2010).
27. Miralles, F., Posem, G., Zaromytidou, A. I. & Treisman, R. Actin dynamics control SRF activity by regulation of its coactivator MAL. *Cell* **113,** 329–342 (2003).
28. Vartiainen, M. K., Guettler, S., Larijiani, B. & Treisman, R. Nuclear actin regulates dynamic subcellular localization and activity of the SRF cofactor MAL. *Science* **316,** 1749–1752 (2007).
29. Yin, J. W. *et al.* Mediator MED23 plays opposing roles in directing smooth muscle cell and adipocyte differentiation. *Genes Dev.* **26,** 2192–2205 (2012).
30. Lyubimova, A., Bershadsky, A. D. & Ben-Ze'ev, A. Autoregulation of actin synthesis responds to monomeric actin levels. *J. Cell Biochem.* **65,** 469–478 (1997).
31. Bubb, M. R., Spector, I., Bershadsky, A. D. & Korn, E. D. Swinholide A is a microfilament disrupting marine toxin that stabilizes actin dimmers and severs actin filaments. *J. Biol. Chem.* **270,** 3463–3466 (1995).
32. Cen, B. *et al.* Megakaryoblastic leukemia 1, a potent transcriptional coactivator for serum response factor (SRF), is required for serum induction of SRF target genes. *Mol. Cell Biol.* **23,** 6597–6608 (2003).
33. Guettler, S., Vartiainen, M. K., Miralles, F., Larijani, B. & Treisman, R. RPEL motifs link the serum response factor cofactor MAL but not myocardin to Rho signaling *via* actin binding. *Mol. Cell Biol.* **28,** 732–742 (2008).
34. Sun, Y. *et al.* Acute myeloid leukemia-associated Mkl1 (Mrtf-a) is a key regulator of mammary gland function. *Mol. Cell Biol.* **26,** 5809–5826 (2006).
35. Liu, J. *et al.* Changes in integrin expression during adipocyte differentiation. *Cell Metab.* **2,** 165–177 (2005).
36. Vassaux, G., Gaillard, D., Ailhaud, G. & Négrel, R. Prostacyclin is a specific effector of adipose cell differentiation. Its dual role as a cAMP- and $Ca^{2+}$-elevating agent. *J. Biol. Chem.* **267,** 11092–11097 (1992).
37. Petersen, R. K. *et al.* Cyclic AMP (cAMP)-mediated stimulation of adipocyte differentiation requires the synergistic action of Epac- and cAMP-dependent protein kinase-dependent processes. *Mol. Cell Biol.* **28,** 3804–3816 (2008).
38. Kawazu, M. *et al.* Transforming mutations of RAC guanosine triphosphatases in human cancers. *Proc. Natl Acad. Sci. USA* **110,** 3029–3034 (2013).
39. Amano, M. *et al.* Identification of a putative target for Rho as the serine-threonine kinase protein kinase N. *Science* **271,** 648–650 (1996).
40. Shimizu, T. *et al.* c-MYC overexpression with loss of Ink4a/Arf transforms bone marrow stromal cells into osteosarcoma accompanied by loss of adipogenesis. *Oncogene* **29,** 5687–5699 (2010).

41. Fujino, R. S. *et al.* Spermatogonial cell-mediated activation of an IκBζ-independent nuclear factor-κB pathway in Sertoli cells induces transcription of the lipocalin-2 gene. *Mol. Endocrinol.* **20,** 904–915 (2006).
42. Kitagawa, M., Fung, S. Y., Onishi, N., Saya, H. & Lee, S. H. Targeting Aurora B to the equatorial cortex by MKlp2 is required for cytokinesis. *PLoS One* **8,** e64826 (2013).
43. Eilers, M., Picard, D., Yamamoto, K. R. & Bishop, J. M. Chimaeras of Myc oncoprotein and steroid receptors cause hormone-dependent transformation of cells. *Nature* **340,** 66–68 (1989).
44. Morita, T., Kojima, T. & Kitamura, T. Plat-E: an efficient and stable system for transient packaging of retroviruses. *Gene Ther.* **7,** 1063–1066 (2000).

## Acknowledgements

We thank T. Hara for the retroviral expression vector pRePS; T. Kitamura for the retroviral expression vector pMXs-puro; O. Sampetrean, S. Kuninaka, and H. Naoe for discussion; RM. Yonamine, X. Wang, H. Ito, N. Yanagihara, and N. Hirose for technical assistance; and K. Arai for secretarial assistance. We are grateful to the Collaborative Research Resources, School of Medicine, Keio University for technical support and reagents. This work was partly supported by a grant from the Ministry of Education, Science, Sports, and Culture of Japan (HS) and a grant from Okinawa Research and Industrialization for the Forefront Medical Care (KK).

## Author contributions

H.N. performed most of the experimental works and wrote the manuscript. N.O. helped experimental design and contributed to the writing of the manuscript. T.S., E.S., Y.O., Y.S., T.C and K.A. helped with the experiments and to review the manuscript prior to submission. H.S. and K.K. supervised the project and manuscript editing, and prepared the manuscript.

## Additional information

**Accession codes:** The raw and processed microarray data have been deposited in the Gene Expression Omnibus under the accession code GSE52334.

**Supplementary Information** accompanies this paper at http://www.nature.com/nature communications

**Competing financial interests:** The authors declare no competing financial interests.

**Reprints and permission** information is available online at http://npg.nature.com/reprintsandpermissions/

**How to cite this article:** Nobusue, H. *et al.* Regulation of MKL1 *via* actin cytoskeleton dynamics drives adipocyte differentiation. *Nat. Commun.* 5:3368 doi: 10.1038/ncomms4368 (2014).

*Journal of Reproduction and Development, Vol. 60, No 3, 2014*

—Original Article—

# Transgenic Pigs with Pancreas-specific Expression of Green Fluorescent Protein

**Hitomi MATSUNARI[1–3], Toshihiro KOBAYASHI[3,4]#, Masahito WATANABE[1,2], Kazuhiro UMEYAMA[1,2], Kazuaki NAKANO[2], Takahiro KANAI[2], Taisuke MATSUDA[2], Masaki NAGAYA[1,2], Manami HARA[5], Hiromitsu NAKAUCHI[3,4] and Hiroshi NAGASHIMA[1–3]**

[1]*Meiji University International Institute for Bio-Resource Research, Kawasaki 214-8571, Japan*
[2]*Laboratory of Developmental Engineering, Department of Life Sciences, School of Agriculture, Meiji University, Kawasaki 214-8571, Japan*
[3]*Nakauchi Stem Cell and Organ Regeneration Project, ERATO, Japan Science and Technology Agency, Tokyo 102-0075, Japan*
[4]*Division of Stem Cell Therapy, Center for Stem Cell Biology and Medicine, Institute of Medical Science, The University of Tokyo, Tokyo 108-8639, Japan*
[5]*Department of Medicine, The University of Chicago, IL 60637, USA*
#*Present: Wellcome Trust /Cancer Research UK Gurdon Institute, University of Cambridge, Cambridge CB2 1QN, UK*

**Abstract.** The development and regeneration of the pancreas is of considerable interest because of the role of these processes in pancreatic diseases, such as diabetes. Here, we sought to develop a large animal model in which the pancreatic cell lineage could be tracked. The pancreatic and duodenal homeobox-1 (*Pdx1*) gene promoter was conjugated to Venus, a green fluorescent protein, and introduced into 370 *in vitro*-matured porcine oocytes by intracytoplasmic sperm injection-mediated gene transfer. These oocytes were transferred into four recipient gilts, all of which became pregnant. Three gilts were sacrificed at 47–65 days of gestation, and the fourth was allowed to farrow. Seven of 16 fetuses obtained were transgenic (Tg) and exhibited pancreas-specific green fluorescence. The fourth recipient gilt produced a litter of six piglets, two of which were Tg. The founder Tg offspring matured normally and produced healthy first-generation (G1) progeny. A postweaning autopsy of four 27-day-old G1 Tg piglets confirmed the pancreas-specific Venus expression. Immunostaining of the pancreatic tissue indicated the transgene was expressed in β-cells. Pancreatic islets from Tg pigs were transplanted under the renal capsules of NOD/SCID mice and expressed fluorescence up to one month after transplantation. Tg G1 pigs developed normally and had blood glucose levels within the normal range. Insulin levels before and after sexual maturity were within normal ranges, as were other blood biochemistry parameters, indicating that pancreatic function was normal. We conclude that *Pdx1-Venus* Tg pigs represent a large animal model suitable for research on pancreatic development/regeneration and diabetes.
**Key words:** ICSI-mediated gene transfer, Pancreas generation, Pdx1, Transgenic pig, Venus

(**J. Reprod. Dev. 60:** 230–237, 2014)

The development and utilization of genetically modified pigs have contributed to the expansion of many biomedical research efforts. For example, genetically modified pigs serving as disease models for retinitis pigmentosa [1], diabetes [2, 3], and cystic fibrosis [4, 5] have been produced, and these models are expected to further the development of new drugs and treatment methods. In xenotransplantation research, α1,3-galactosyltransferase gene knockout pigs and pigs carrying human complement regulatory factor genes have been produced (for review, see [6, 7]) and are now being used in preclinical experiments, such as the transplantation of swine organs to monkeys. Additionally, pigs expressing fluorescent proteins are exceptionally useful in research on topics such as cell tracking [8, 9] and tissue regeneration [10]. Even more innovative and more widely applicable research results are likely to be obtained through the future use of genetically modified pigs. The aim of our research was to produce transgenic (Tg) pigs to advance research on pancreas generation.

Overcoming diabetes is a global challenge for modern society; thus, the production of Tg pigs that can be used to understand the mechanisms underlying pancreatic development and the control of pancreatic functions is of great value. We therefore embarked on a program to produce Tg pigs that express the Venus variant of green fluorescent protein (GFP) [11] under the control of the pancreatic duodenal homeobox-1 (*Pdx1*) gene promoter. *Pdx1* functions as a master gene that induces the differentiation of β-cells from pancreatic stem cells, and research on Pdx1-positive cells is important for understanding the development of the pancreas and β-cell differentiation [12, 13]. The study of Pdx1-positive pancreatic stem cells may also lead to improved pathophysiological analysis and the development of treatments [13].

Methods for producing Tg pigs include pronuclear DNA injection [14], somatic cell nuclear transfer [15] and intracytoplasmic

Received: January 14, 2014
Accepted: March 11, 2014
Published online in J-STAGE: April 21, 2014

Correspondence: H Nagashima (hnagas@isc.meiji.ac.jp)

sperm injection-mediated gene transfer (ICSI-MGT) [16]. We chose ICSI-MGT for the present study, having previously confirmed that ICSI-MGT to *in vitro*-matured (IVM) porcine oocytes enables the production of Tg pigs with a high potential for reproducibility [2, 17].

In the present study, we first produced several Tg pig fetuses by ICSI-MGT to confirm that the transferred *Pdx1-Venus* gene was expressed exclusively in the pancreas. Then, we produced Tg pigs and examined their progeny to determine whether the genes were transmitted to the succeeding generation, confirming the reproducibility of the pattern of pancreas-specific expression. We further transplanted pancreatic islets of the *Pdx1-Venus* Tg pig to immunodeficient mice to verify their *in vivo* traceability. The utility of the *Pdx1-Venus* Tg pigs as a model for research on pancreatic development is discussed.

## Materials and Methods

### *Animal care*

All animal experiments in this study were approved by the Institutional Animal Care and Use Committee of Meiji University (IACUC-07-0005).

### *Chemicals*

All chemicals were purchased from the Sigma Aldrich Chemical (St. Louis, MO, USA) unless otherwise indicated.

### *Construction of the Pdx1-Venus transgene*

The *Pdx1-Venus* transgene construct (8.4 kb) consisted of the mouse *Pdx1* promoter, *Venus* cDNA, and rabbit β-globin gene sequence (from partway through the second exon to the 3' untranslated region), including a polyadenylation signal (pA) (Fig. 1). The transgene fragment was excised from the plasmid vector by enzymatic digestion using the *Bss*HII restriction enzyme (Takara Bio, Shiga, Japan), separated by gel electrophoresis, and purified using the QIAquick® Gel Extraction Kit (QIAGEN, Hilden, Germany).

### *In vitro maturation of oocytes*

Porcine ovaries were collected at a local abattoir and transported to the laboratory in Dulbecco's phosphate buffered saline (DPBS, Nissui Pharmaceutical, Tokyo, Japan) containing 75 μg/ml potassium penicillin G, 50 μg/ml streptomycin sulfate, 2.5 μg/ml amphotericin B, and 0.1% (w/v) polyvinyl alcohol (PVA). Cumulus-oocyte complexes were collected from the ovarian antral follicles (3.0 to 6.0 mm in diameter) by aspiration with a 10-ml syringe and a 20 G hypodermic needle, and those with at least three layers of compacted cumulus cells were selected and cultured in NCSU23 medium [18] supplemented with 0.6 mM cysteine, 10 ng/ml epidermal growth factor, 10% (v/v) porcine follicular fluid, 75 μg/ml potassium penicillin G, 50 μg/ml streptomycin sulfate, 10 IU/ml eCG (ASKA Pharmaceutica, Tokyo, Japan), and 10 IU/ml hCG (ASKA Pharmaceutical) at 38.5 C in a humidified atmosphere of 5% $CO_2$ in air for 22 h. Then, the oocytes were cultured for an additional 21 h without eCG and hCG at 38.5 C in a humidified atmosphere of 5% $CO_2$, 5% $O_2$, and 90% $N_2$ [19]. IVM oocytes with expanded cumulus cells were treated with 1 mg/ml hyaluronidase dissolved in Tyrode lactose medium containing 10 mM HEPES and 0.3% (w/v) polyvinylpyrrolidone (TL-HEPES-PVP) and separated from the cumulus cells by gentle pipetting. Oocytes with an evenly granulated ooplasm and an extruded first polar body were selected for the subsequent experiments.

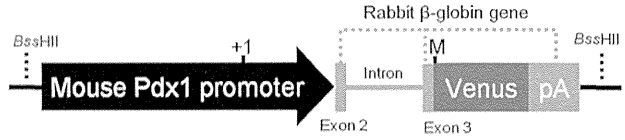


**Fig. 1.** Structure of an expression vector for the *Pdx1-Venus* cDNA. A schematic presentation of the *Pdx1-Venus* transgene used to generate transgenic pigs. The fusion gene (8.4 kb) consists of 6.5 kb of the mouse Pdx1 promoter and a rabbit β-globin gene including an insertion of 0.72 kb Venus cDNA in the 3rd exon and a polyadenylation signal in the 3' -flanking region. Transcription and translation start site are indicated by +1 and M, respectively.

### *Porcine sperm preparation for ICSI-MGT*

Commercially available boar semen (Duroc) suitable for artificial insemination was used to prepare frozen sperm for ICSI-MGT. Beltsville thawing solution (BTS) was used as a freezing solution without cryoprotective agents [20]. The sperm were washed three times by centrifugation at 200 × *g* for 5 min in BTS to remove the extender. The sperm were then suspended in BTS (containing 5% (w/v) BSA) at a concentration of $3 \times 10^7$ cells/ml, placed in 0.25-ml plastic freezing straws (Fujihira Industry, Tokyo, Japan), and plunged into liquid nitrogen. The straws of frozen sperm were thawed by soaking in a 37 C water bath for 10 sec. The sperm recovered from the straws were washed twice in BTS (containing 0.1% (w/v) BSA), suspended in Nucleus Isolation Medium (NIM) [21], and used in ICSI-MGT within 60 min of thawing. For tail removal by sonication, an ultrasonic sonicator (Honda Electronics, Aichi, Japan) was used to apply ultrasonic vibrations (100 W, 28 kHz) for 9 sec to 300 μl of the sperm suspension ($5 \times 10^7$ cells/ml) in a 1.5-ml microcentrifuge tube. This duration of sonication was determined to decapitate approximately 70% of the sperm. Sperm that had been subjected to tail removal by sonication were resuspended in NIM at a concentration of $2–5 \times 10^4$ cells/μl. Next, the DNA solution was added to the sperm suspension to yield a concentration of 2.5 ng/μl. The suspension was then gently mixed and incubated at room temperature for 5 min. The resulting sperm were stored on ice until use in ICSI-MGT.

### *Intracytoplasmic sperm injection*

The IVM oocytes at 43–45 h after commencement of the maturation culture were activated by electrical stimulation before the injection of sperm heads. The oocytes were lined up between two wire electrodes (1.0 mm apart) of a fusion chamber (CUY500G1, Nepa Gene, Chiba, Japan) and overlaid with an activation solution, consisting of 0.28 M mannitol (Nacalai Tesque, Kyoto, Japan), 50 μM $CaCl_2$, 100 μM $MgSO_4$, and 0.01% (w/v) PVA. Activation was induced with one DC pulse of 150 V/mm for 100 μsec using an electric pulsing machine (ET-1, Fujihira Industry).

ICSI-MGT was performed in a 4-μl drop of TL-HEPES-PVP under mineral oil using an Nikon inverted microscope (TE-300,

Nikon, Tokyo, Japan) as described previously [17]. Approximately 1 μl of sperm suspension that had been co-incubated with DNA was transferred to a 2-μl drop of 10% (w/v) PVP (in DPBS; Irvine Scientific, Sales, Santa Ana, CA, USA). Sperm heads were aspirated from the PVP drop using an injection pipette and moved to the drop containing the oocytes. An oocyte was first captured by a holding pipette. Next, with the oocyte immobilized with its polar body at either the 6- or 12-o'clock position, a sperm head was injected using the piezo-actuated microinjection unit (PMM-150FU, Prime Tech, Tsuchiura, Japan) and micromanipulators (MO-202U, Narishige, Tokyo, Japan). Sperm injection was carried out within 30 min of activation of the oocytes.

After ICSI-MGT, embryos to be transferred to recipients were cultured in Porcine Zygote Medium-5 (PZM-5, Research Institute for the Functional Peptides, Yamagata, Japan) for 1–3 days under a humidified atmosphere of 5% $CO_2$, 5% $O_2$, and 90% $N_2$ at 38.5 C.

*Embryo transfer*

Crossbred (Large White/Landrace × Duroc) prepubertal gilts weighing from 100 to 105 kg were used as recipients of the sperm-injected embryos. The gilts were treated with a single intramuscular injection of 1000 IU of eCG to induce estrus. Ovulation was induced by an intramuscular injection of 1500 IU of hCG (Kawasaki Pharmaceutical, Kanagawa, Japan) given 66 h after the injection of eCG. Sperm-injected embryos cultured for 1–3 days were surgically transferred into the oviducts of recipients approximately 48 h or 72 h after hCG injection.

All but one of the pregnant recipients were laparotomized to recover fetuses at 47–65 days of gestation, and the remaining recipient was allowed to farrow.

*PCR and Southern blot analyses*

Genomic DNA was extracted from tail biopsies of fetuses and newborn piglets using proteinase K (Life Technologies Corporation, Carlsbad, CA, USA) and purified by the phenol-chloroform method. To identify Tg pigs, DNA samples were analyzed by PCR using the following primers: 5'-caatgatggctccagggtaa (forward) and 5'-ctccttgaagtcgatgccctt (reverse).

For Southern blot analysis, genomic DNA extracted as described above was digested with the *PstI* restriction enzyme (Takara Bio), separated by gel electrophoresis, and transferred onto a nylon membrane (GE Healthcare, Buckinghamshire, UK), which was then hybridized with the DIG-labeled probes prepared by PCR using the following primers: 5'-caatgatggctccagggtaa (forward) and 5'-ggtggtgcagatcagcttca (reverse). The signal (i.e., binding of the probe) was detected by chromogenic methods. The number of transgene copies integrated into the porcine genome was determined by comparison of the hybridization signal with that of the copy-number control, which was diluted to make a standard series (1–100 copies per diploid genome).

*Pancreas-specific fluorescence expression in Tg fetuses and G1 offspring*

The tails of the fetuses (day 47–65) obtained from autopsies of the sacrificed pregnant pigs were used to extract genomic DNA. Tg fetuses were identified by PCR. Fetal viscera were also removed, and the expression of green fluorescence in the organs was analyzed by fluorescence stereomicroscopy (MVX10, Olympus, Tokyo, Japan; excitation wavelength of 460–480 nm; absorption filter of 495–540 nm). Pancreatic tissue samples from fetuses were fixed in 4% paraformaldehyde and used to prepare paraffin-embedded sections (hematoxylin/eosin stain). The paraffin-embedded sections were also analyzed by fluorescence microscopy (Olympus BX52; excitation wavelength of 460–480 nm; absorption filter of 495–540 nm).

A subset of the founder Tg pigs was allowed to grow to maturity and was mated with wild-type pigs. The offspring (G1) obtained were sacrificed when they reached the age of 27 days to examine pancreas-specific fluorescence expression by fluorescence stereomicroscopy.

Pancreatic tissue samples of the founder Tg pig (G0) were double-stained using anti-insulin (1:500; LS-C24686, LifeSpan BioSciences, Seattle, WA, USA) and anti-GFP (1:500-1:1000; #598, MBL, Nagoya, Japan) antibodies to determine the Venus-expressing cells in the pancreatic islets. Alexa Fluor® 594 goat anti-guinea pig IgG (A11076, Life Technologies) and Alexa Fluor® 488 donkey anti-rabbit IgG (A21206, Life Technologies) were used as the secondary antibodies. The tissue sections were also double-stained for glucagon and Venus. For glucagon staining, anti-glucagon antibody (1:500; G2654) and Alexa Fluor®594 goat anti-mouse IgG (A11020, Life Technologies) were employed. After antibody treatments, the sections were mounted in Vectashield mounting medium (Vector Laboratories, Burlingame, CA, USA) containing 4′,6-diamidino-2-phenylindole (DAPI) for nuclear counterstaining and observed by confocal laser scanning microscopy (FV1000-D; Olympus, Tokyo, Japan).

*Fluorescence in situ hybridization (FISH)*

Peripheral blood cells derived from the two Tg founder pigs (male and female) were cultured in RPMI1640 containing 20% (v/v) FBS for 3 days. The cells were then cultured with 30 μg/ml BrdU for 5 h, followed by incubation with 0.02 μg/ml colcemide for 1 h. After fixation with methanol-acetic acid (3:1 ratio), the cells were spread on slides and air-dried. The cells were then stained with Hoechst 33258 and treated with UV light for G-banding. *Pdx1-Venus* DNA was labeled with Cy3 as a probe and hybridized at 37 C overnight. After stringent washing, the bound label was detected with anti–Dig-Cy3 using Leica DRAM2 and CW4000 FISH software.

*Tracing of pancreatic islets by fluorescence after ectopic transplantation*

Pancreatic islets were isolated from a 4.5-month-old Tg pig using a conventional method. The pancreas collected from a Tg pig was distended by infusion with Liberase DL (Roche Diagnostics, Indianapolis, IN, USA) suspended in Hank's balanced salt solution (HBSS; Life Technologies), followed by a static incubation in an empty 125 ml storage bottle for 30 min at 37 C. Then the digesting pancreatic tissue was gently shaken with 7 mm Teflon® beads in RPMI 1640 (Life Technologies). Digestion was terminated by the addition of cold HBSS containing 10% (v/v) FBS, 100 IU/ml of penicillin, 100 mg/ml of streptomycin, and 2.5 μg/ml amphotericin B. The digested tissue was passed through a 500 μm stainless steel mesh screen. The tissue effluent was collected in 50 ml conical tubes and centrifuged for 2 min at 155 × *g* at 4 C. The islets were purified using a Histopaque®-1.077 gradient with RPMI 1640. Following

**Table 1.** Efficiency of the ICSI-MGT method for the production of Tg pig fetuses and offspring carrying the *Pdx1-Venus* gene

| | Recipient | No. of embryos transferred | Production efficiency of fetuses or offspring (%)*1 | Production efficiency of Tg fetuses or offspring (%)*2 |
|---|---|---|---|---|
| Fetus | W8 | 83 | 8.4 [7/83] | 28.6 [2/7] |
| | W9 | 81 | 3.7 [3/81] | 100 [3/3] |
| | W11 | 79 | 7.6 [6/79] | 33.3 [2/6] |
| Offspring | W10 | 127 | 4.7 [6/127] | 33.3 [2/6] |

*1 No. of fetuses or piglets / No. of embryos transferred × 100. *2 No. of Tg fetuses or piglets / No. of fetuses or piglets obtained × 100.

**Table 2.** Expression of the *Pdx1-Venus* gene in Tg pig fetuses produced by the ICSI-MGT method

| Fetus | Fetal age | Fetal sex | Fluorescence intensity | Transgene copy number |
|---|---|---|---|---|
| W8-1 | Day 48 | F | + | 30 |
| W8-5 | Day 48 | F | + | 5 |
| W9-1 | Day 47 | F | + | 5 |
| W9-2 | Day 47 | M | ++ | 15 |
| W9-3 | Day 47 | M | ++ | 70 |
| W11-2 | Day 65 | F | + | 5 |
| W11-5 | Day 65 | F | ++ | 100≤ |

centrifugation at 1700 × *g* for 17 min at 4 C, the islets were collected from the interface between the RPMI 1640 and Histopaque®-1.077. Purified islets were washed by centrifugation at 155 × *g* for 2 min at 4 C in RPMI 1640 supplemented with 10% (v/v) FBS. The purity of the isolated islets was confirmed to be over 90% by microscopic inspection after Dithizone (5 mg/ml, in DPBS) staining.

Fluorescence in the isolated islets was observed by fluorescence stereoscopic microscopy (MVX10, Olympus). Isolated islets were then transplanted under the renal capsules of anesthetized NOD/SCID mice (CLEA Japan, Tokyo, Japan). Kidneys were removed either immediately or at one month after transplantation and analyzed by fluorescence stereomicroscopy (MVX10, Olympus) to determine whether the islets could be traced using Venus fluorescence as an indicator.

## Results

*Efficiency of production of Pdx1-Venus Tg pigs by ICSI-MGT*

The ICSI-MGT method was selected for creating *Pdx1-Venus* Tg pigs. In total, 370 sperm-injected embryos were transferred into four recipients, all of which became pregnant.

Three of the recipient pigs were autopsied at 47–65 days of gestation, and 16 fetuses were recovered for analysis (Table 1). The production efficiency of fetuses was between 4 and 8%, as each recipient received approximately 80 embryos. Seven of the 16 fetuses were Tg (43.8%), including approximately 30% of the fetuses in two of the recipients and all three fetuses in one recipient. Overall, 2.4–3.7% of the transferred embryos produced Tg fetuses.

The fourth pregnant pig, which received 127 embryos, was allowed to farrow and produced six (4.7%) piglets, two of which were Tg (one female and one male).

*Pancreas-specific expression of Venus in Tg fetuses and offspring*

The viscera of the seven Tg fetuses obtained were examined by fluorescence stereomicroscopy, and we found that all the fetuses had pancreas-specific expression of Venus fluorescence (Fig. 2A and B). The Southern blot analysis of genomic DNAs indicated an integration of 5 to 100 copies of the gene. Although the fluorescence intensity tended to be greater in fetuses with higher copy numbers (≥15), except for a female fetus (W8-1) harboring 30 copies of the gene, pancreas-specific expression was clear in all fetuses regardless of the copy number (Table 2).

A histological analysis of pancreatic tissues of four Tg fetuses showed that Venus fluorescence was present in cells determined to be acinar cells based on their appearance. This expression pattern was consistent among all fetuses analyzed (Fig. 2C and D).

The two founder (G0; male and female) Tg pigs grew normally to adulthood and were crossed with wild-type pigs to produce G1 offspring of six litters. Of the 22 G1 pigs obtained from the male founder and the 28 G1 pigs derived from the female founder, the transgene was transmitted to 10 (45.5%) and 16 pigs (57.1%), respectively, indicating that the transgene was transmitted in the Mendelian fashion. It was found that 10 and 30 transgene copies were integrated into the genomes of the male and female founder pigs, respectively. FISH analysis of these founder Tg pigs revealed that concatemerized transgenes were integrated into a single site on the chromosomes (Suppl. Fig. 1: on-line only).

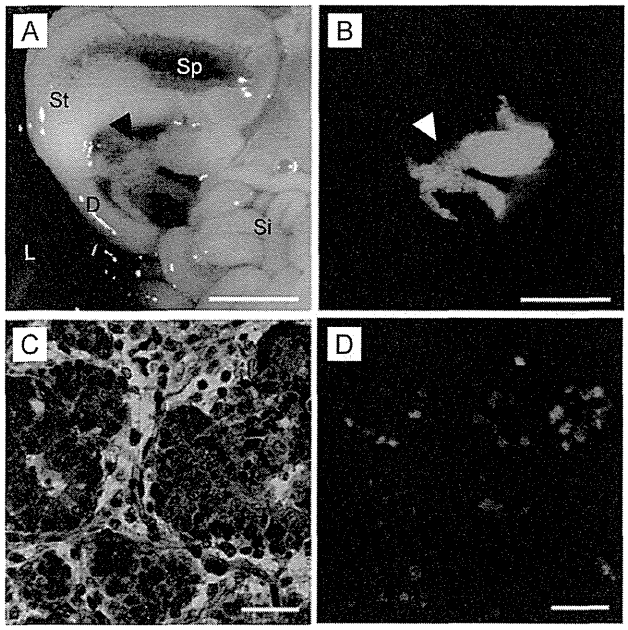


**Fig. 2.** Pancreas-specific expression of the *Pdx1-Venus* gene in the Tg pig fetus. Bright-field (A) and fluorescence microscopic (B) observation of the pancreas (arrowheads). Acinar cells (C, HE stain) showed prominent Venus expression (D). D, duodenum; L, liver; Si, small intestine; Sp, spleen; St, stomach. Scale bars = 5 mm (A, B); 50 μm (C, D).

Four 27-day-old G1 piglets (Tg female and male, non-Tg female and male) were autopsied to examine fluorescence expression in their viscera. The pancreas, duodenum, small intestine, liver, spleen, kidneys, skin, heart, lungs, and stomach were observed under a fluorescence stereomicroscope. This analysis confirmed the retention of pancreas-specific fluorescence expression (Fig. 3A and Suppl. Fig. 2: on-line only) as in the founder Tg fetuses. Green fluorescence was not detected in the viscera of non-Tg pigs.

The pancreatic tissue of the G1 Tg pigs showed green fluorescent spots throughout (Fig. 3A), indicating *Pdx1-Venus* expression in islets. Venus expression was found to be confined to β-cells in the pancreatic tissue after double staining with anti-insulin and anti-GFP antibodies (Fig. 3B).

### *Tracing of the fluorescence expression of pancreatic islets*

To further examine the potential of *Pdx1-Venus* Tg pigs for future use in pancreatic islet research, we investigated the traceability of the pancreatic islets using their fluorescence as an indicator. As shown in Fig. 4, Venus fluorescence expression patterns were clearly observed under a fluorescence stereomicroscope, which confirmed clear fluorescence spots in the islets (Fig. 4A and A').

The isolated islets were transplanted under the renal capsules of NOD/SCID mice, and the transplanted islets could clearly be identified by their fluorescence. The fluorescence of the transplanted pancreatic islets was still clear at 30 days after transplantation (Fig. 4C and C').

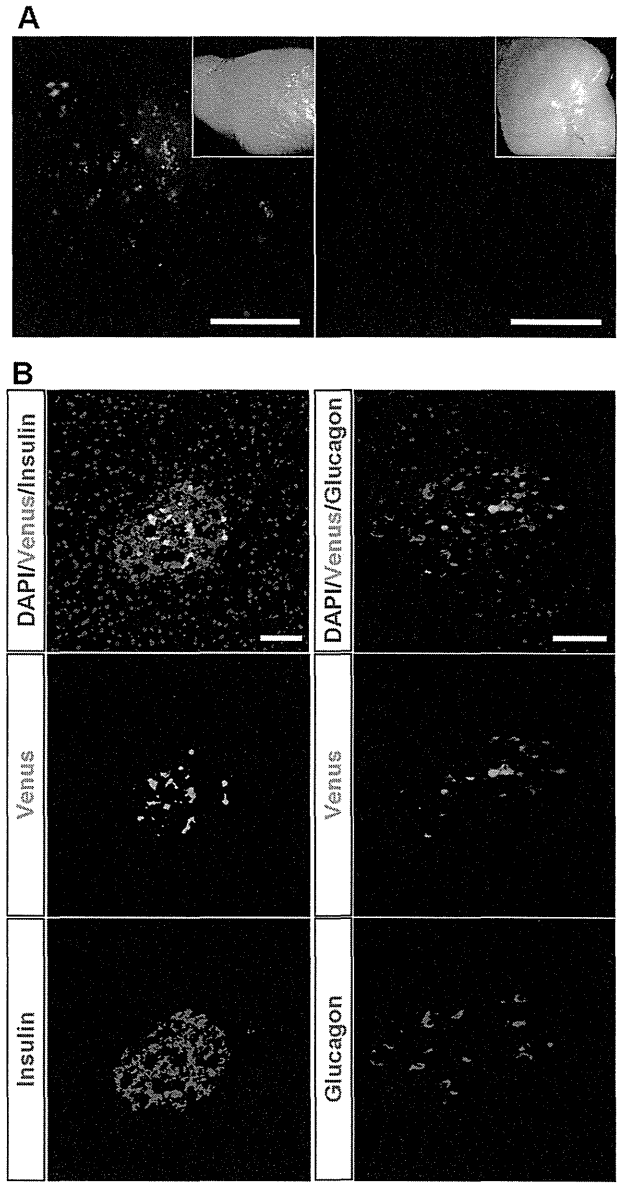


**Fig. 3.** Expression of the *Pdx1-Venus* gene in the pancreas of a Tg pig. (A) Green fluorescent spots were observed by fluorescence stereomicroscopy throughout the pancreatic tissue of the Tg pigs (left panel), indicating *Pdx1-Venus* expression in islets. Right panel: pancreatic tissue of a control wild-type pig. The inset in each panel presents a bright-field image of the tissue. Scale bars = 2.5 mm. (B) Immunohistochemical staining of pancreatic islets of a *Pdx1-Venus* Tg pig. Merged images of the Tg pig islet demonstrated that the expression of the *Pdx1-Venus* gene was confined to β-cells (top left), whereas this gene was not expressed in glucagon-producing cells (top right). Scale bars = 50 μm.

## Discussion

This report describes the production of the first *Pdx1-Venus* Tg pig expressing green fluorescent protein specifically in the pancreas,

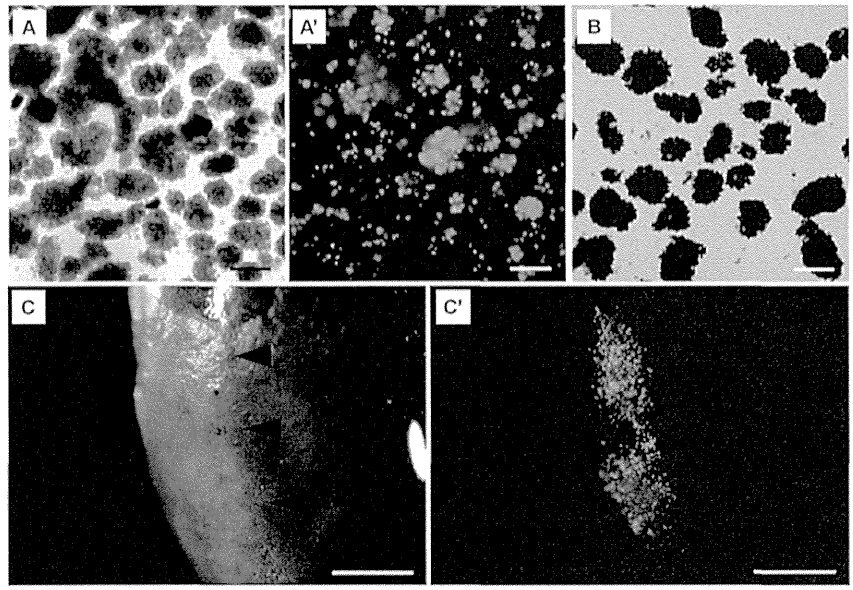


**Fig. 4.** Fluorescence of pancreatic islets isolated from a *Pdx1-Venus* Tg pig. (A) Pancreatic islets isolated from a Tg pig. (A') Fluorescent spots were observed in the islets of a Tg pig. (B) Dithizone-stained islets of a Tg pig. (C, C') Pancreatic islets of a *Pdx1-Venus* Tg pig transplanted into the kidney capsule of NOD/SCID mice (arrowheads). Bright-field (C) and fluorescence (C') observation by fluorescence stereomicroscopy showed that the fluorescence of the transplanted islets was clear at 30 days after transplantation (A'). Scale bars = 200 μm (A–C); 1 mm (C, C').

particularly in β-cells. Pdx1 is a key molecule with an important role in pancreatic stem cell differentiation into β-cells [12, 13, 22, 23]. In fact, *Pdx1* knockout mice reportedly suffer impaired pancreatic development [12, 24]. The identification and separation of *Pdx1*-positive cells is therefore expected to stimulate new developments in research on islet architecture during the ontogeny and differentiation of β-cells from precursors [13, 25, 26]. Research on pancreas development and β-cell differentiation is also expected to lead to the pathophysiological analysis of diabetes and the development of new therapeutic methods [27]. In particular, the neogenesis of β-cells has been a recent focus in diabetes research [28–31].

In research using laboratory rodents, $Pdx1^{GFP/w}$ mice [32] and mouse insulin I gene promoter (MIP)-GFP Tg mice [33] have been created and used to conduct research on pancreatic development and differentiation. However, in research using pigs, a Tg model that is useful for the study of β-cell biology, including the identification of progenitor cells, has not been available. Considering that the importance of pigs, as a large laboratory animal with several similarities to humans, in translational research is now recognized and that research is being undertaken on the clinical applications of porcine islet transplantation [34], the *Pdx1-Venus* pig we have produced has strong potential for use as an effective research tool. The Expression pattern of the *Pdx1-Venus* in the islet of our transgenic pigs was similar to that reported previously in the $Pdx1^{GFP/w}$ mice [32].

In the present study, we employed the mouse *Pdx1* promoter to drive the *Venus* expression in the transgenic pigs. However the transgene was expressed in a highly tissue-specific manner. In fact, *Pdx1-Venus* expression was confined to the pancreas during the early fetal stage (day 47) and at the adult stage. *Pdx1* is also known to be expressed in the duodenum at the fetal stage [13]. Further studies need to be undertaken to examine the expression of the *Pdx1-Venus* in the early stages of pancreatogenesis in the transgenic pig fetuses.

Concerning *Pdx1-Venus* expression in the islets, we observed that cells that were Venus positive were also insulin-positive cells. This pig is, accordingly, very useful for tracking the behavior of pancreatic progenitor cells and β-cells.

*Pdx1-Venus* is also useful as a cell marker following islet transplantation. The clinical application of islet transplantation using human islets has been hampered, as is the case with other transplants, by the shortage of donor organs. However, if xenogeneic pancreas transplantation—more specifically, the transplantation of pig islets to humans—becomes possible, substantial advances will be made in treatments for diabetes patients [35]. Xenogeneic transplantation will require further basic studies, including a long-term follow-up of islets transplanted to animals. *Pdx1-Venus* Tg pig islets will serve as a very useful tool in such research. For example, production of insulin or C-peptide from the transplanted islets may be correlated with the *Pdx1-Venus* expression that indicates the viability of β-cells. We have already produced diabetic model Tg pigs by mutant hepatocyte nuclear factor-1α gene transfer [2]. Transplanting islets from *Pdx1-Venus* Tg pigs using such diabetic models should provide knowledge that can be extrapolated from large animals to humans.

*Pdx1-Venus* Tg pigs were observed to show a high level of green fluorescence expression in the pancreas (β-cells) with normal pancreas

function. This finding was confirmed by the pigs' physiological characteristics, including growth, casual blood glucose levels, postprandial blood glucose and insulin levels, and blood biochemical parameters, which were measured during the period from the postweaning through the growth stages (Suppl. Text, Suppl. Fig. 3, and Suppl. Table 1: on-line only). Based on these results, we hypothesize that *Pdx1-Venus* Tg pigs may also be suitable as donor animals in studies of islet transplantation.

In this study, we introduced transgenes using the ICSI-MGT method. We previously reported that the application of ICSI-MGT is highly effective for introducing exogenous genes to porcine IVM oocytes [2, 17]. In this study, approximately 30–100% of the fetuses/piglets obtained in each litter were Tg, once more demonstrating the high efficiency of the ICSI-MGT method. The production efficiency of Tg fetuses or piglets obtained in this study was equal or rather higher compared with our previous studies, probably due to lower detrimental effect of the transgene expression [2, 36, 37]. *In vitro* maturation of pig oocytes is now an established method, and the combination of IVM oocytes and the ICSI-MGT method can accordingly be considered a practical method for generating Tg pigs.

Our previous research confirmed that transgenes introduced by the ICSI-MGT method generally insert into a single site on the host genome as concatemers [17, 38]. In the founder Tg pigs used for generating G1 offspring in this study, it was shown that the transgenes did concatamerize and integrated into a single site of the chromosome as shown in our previous studies [17, 38]. No significant differences in growth were observed in fetuses with transgene copy numbers between 5 and 100. The level of transgene expression is considered to be more readily influenced by the integration site on the chromosome than by the integrated copy number [39, 40]. Even so, in the case of Tg individuals with an exceptionally high number of integrated transgenes, it is possible that high-level transgene expression may influence normality in piglets and affect their long-term survival. Because the copy number of the integrated genes is affected by various factors related to the binding of DNA to sperm [38, 41, 42], the preliminary optimization of the transgene-sperm co-incubation will be critical for the efficient production of Tg pigs using the ICSI-MGT method.

In conclusion, building on our current knowledge, this study verifies that using IVM oocytes and ICSI-MGT together is an effective method for producing Tg pigs. Additionally, because the *Pdx1-Venus* Tg pigs produced in this study express green fluorescent protein specifically in the pancreas (β-cells) and maintain normal physiological function, we can conclude that this large animal model is suitable for research on pancreatic development and regeneration as well as diabetes.

## Acknowledgments

This work was supported by the Japan Science and Technology Agency, ERATO, Nakauchi Stem Cell and Organ Regeneration Project, JSPS KAKENHI Grant Number 24659596, and the Meiji University International Institute for Bio-Resource Research (MUIIBR).

## References

1. **Petters RM, Alexander CA, Wells KD, Collins EB, Sommer JR, Blanton MR, Rojas G, Hao Y, Flowers WL, Banin E, Cideciyan AV, Jacobson SG, Wong F.** Genetically engineered large animal model for studying cone photoreceptor survival and degeneration in retinitis pigmentosa. *Nat Biotechnol* 1997; **15**: 965–970. [Medline] [CrossRef]
2. **Umeyama K, Watanabe M, Saito H, Kurome M, Tohi S, Matsunari H, Miki K, Nagashima H.** Dominant-negative mutant hepatocyte nuclear factor 1alpha induces diabetes in transgenic-cloned pigs. *Transgenic Res* 2009; **18**: 697–706. [Medline] [CrossRef]
3. **Renner S, Fehlings C, Herbach N, Hofmann A, von Waldthausen DC, Kessler B, Ulrichs K, Chodnevskaja I, Moskalenko V, Amselgruber W, Göke B, Pfeifer A, Wanke R, Wolf E.** Glucose intolerance and reduced proliferation of pancreatic beta-cells in transgenic pigs with impaired glucose-dependent insulinotropic polypeptide function. *Diabetes* 2010; **59**: 1228–1238. [Medline] [CrossRef]
4. **Rogers CS, Stoltz DA, Meyerholz DK, Ostedgaard LS, Rokhlina T, Taft PJ, Rogan MP, Pezzulo AA, Karp PH, Itani OA, Kabel AC, Wohlford-Lenane CL, Davis GJ, Hanfland RA, Smith TL, Samuel M, Wax D, Murphy CN, Rieke A, Whitworth K, Uc A, Starner TD, Brogden KA, Shilyansky J, McCray PB Jr, Zabner J, Prather RS, Welsh MJ.** Disruption of the CFTR gene produces a model of cystic fibrosis in newborn pigs. *Science* 2008; **321**: 1837–1841. [Medline] [CrossRef]
5. **Klymiuk N, Mundhenk L, Kraehe K, Wuensch A, Plog S, Emrich D, Langenmayer MC, Stehr M, Holzinger A, Kröner C, Richter A, Kessler B, Kurome M, Eddicks M, Nagashima H, Heinritzi K, Gruber AD, Wolf E.** Sequential targeting of *CFTR* by BAC vectors generates a novel pig model of cystic fibrosis. *J Mol Med (Berl)* 2012; **90**: 597–608. [Medline] [CrossRef]
6. **Miyagawa S, Yamamoto A, Matsunami K, Wang D, Takama Y, Ueno T, Okabe M, Nagashima H, Fukuzawa M.** Complement regulation in the GalT KO era. *Xenotransplantation* 2010; **17**: 11–25. [Medline] [CrossRef]
7. **Matsunari H, Watanabe M, Umeyama K, Nakano K, Kurome M, Kessler B, Wolf E, Miyagawa S, Nagashima H.** Cloning of homozygous α1,3-galactosyltransferase gene knock-out pigs by somatic cell nuclear transfer. In: Miyagawa S (ed.), Xenotransplantation. Rijeka, Croatia: InTech; 2012: 37-54.
8. **Lai L, Park KW, Cheong HT, Kühholzer B, Samuel M, Bonk A, Im GS, Rieke A, Day BN, Murphy CN, Carter DB, Prather RS.** Transgenic pig expressing the enhanced green fluorescent protein produced by nuclear transfer using colchicine-treated fibroblasts as donor cells. *Mol Reprod Dev* 2002; **62**: 300–306. [Medline] [CrossRef]
9. **Matsunari H, Onodera M, Tada N, Mochizuki H, Karasawa S, Haruyama E, Nakayama N, Saito H, Ueno S, Kurome M, Miyawaki A, Nagashima H.** Transgenic-cloned pigs systemically expressing red fluorescent protein, Kusabira-Orange. *Cloning Stem Cells* 2008; **10**: 313–323. [Medline] [CrossRef]
10. **Shigeta T, Hsu HC, Enosawa S, Matsuno N, Kasahara M, Matsunari H, Umeyama K, Watanabe M, Nagashima H.** Transgenic pig expressing the red fluorescent protein kusabira-orange as a novel tool for preclinical studies on hepatocyte transplantation. *Transplant Proc* 2013; **45**: 1808–1810. [Medline] [CrossRef]
11. **Nagai T, Ibata K, Park ES, Kubota M, Mikoshiba K, Miyawaki A.** A variant of yellow fluorescent protein with fast and efficient maturation for cell-biological applications. *Nat Biotechnol* 2002; **20**: 87–90. [Medline] [CrossRef]
12. **Jonsson J, Carlsson L, Edlund T, Edlund H.** Insulin-promoter-factor 1 is required for pancreas development in mice. *Nature* 1994; **371**: 606–609. [Medline] [CrossRef]
13. **Bonal C, Herrera PL.** Genes controlling pancreas ontogeny. *Int J Dev Biol* 2008; **52**: 823–835. [Medline] [CrossRef]
14. **Hammer RE, Pursel VG, Rexroad CEJ Jr, Wall RJ, Bolt DJ, Ebert KM, Palmiter RD, Brinster RL.** Production of transgenic rabbits, sheep and pigs by microinjection. *Nature* 1985; **315**: 680–683. [Medline] [CrossRef]
15. **Park KW, Cheong HT, Lai L, Im GS, Kühholzer B, Bonk A, Samuel M, Rieke A, Day BN, Murphy CN, Carter DB, Prather RS.** Production of nuclear transfer-derived swine that express the enhanced green fluorescent protein. *Anim Biotechnol* 2001; **12**: 173–181. [Medline] [CrossRef]
16. **Yong HY, Hao Y, Lai L, Li R, Murphy CN, Rieke A, Wax D, Samuel M, Prather RS.** Production of a transgenic piglet by a sperm injection technique in which no chemical or physical treatments were used for oocytes or sperm. *Mol Reprod Dev* 2006; **73**: 595–599. [Medline] [CrossRef]
17. **Kurome M, Ueda H, Tomii R, Naruse K, Nagashima H.** Production of transgenic-clone pigs by the combination of ICSI-mediated gene transfer with somatic cell nuclear transfer. *Transgenic Res* 2006; **15**: 229–240. [Medline] [CrossRef]
18. **Petters RM, Wells KD.** Culture of pig embryos. *J Reprod Fertil Suppl* 1993; **48**: 61–73. [Medline]
19. **Funahashi H, Day BN.** Effects of the duration of exposure to hormone supplements on cytoplasmic maturation of pig oocytes in vitro. *J Reprod Fertil* 1993; **98**: 179–185. [Medline] [CrossRef]
20. **Pursel VG, Johnson LA.** Freezing of boar spermatozoa: fertilizing capacity with concen-

trated semen and a new thawing procedure. *J Anim Sci* 1975; **40**: 99–102. [Medline]

21. **Kuretake S, Kimura Y, Hoshi K, Yanagimachi R.** Fertilization and development of mouse oocytes injected with isolated sperm heads. *Biol Reprod* 1996; **55**: 789–795. [Medline] [CrossRef]
22. **Wang H, Maechler P, Ritz-Laser B, Hagenfeldt KA, Ishihara H, Philippe J, Wollheim CB.** Pdx1 level defines pancreatic gene expression pattern and cell lineage differentiation. *J Biol Chem* 2001; **276**: 25279–25286. [Medline] [CrossRef]
23. **Lottmann H, Vanselow J, Hessabi B, Walther R.** The Tet-On system in transgenic mice: inhibition of the mouse pdx-1 gene activity by antisense RNA expression in pancreatic beta-cells. *J Mol Med (Berl)* 2001; **79**: 321–328. [Medline] [CrossRef]
24. **Ahlgren U, Jonsson J, Edlund H.** The morphogenesis of the pancreatic mesenchyme is uncoupled from that of the pancreatic epithelium in IPF1/PDX1-deficient mice. *Development* 1996; **122**: 1409–1416. [Medline]
25. **Holland AM, Hale MA, Kagami H, Hammer RE, MacDonald RJ.** Experimental control of pancreatic development and maintenance. *Proc Natl Acad Sci USA* 2002; **99**: 12236–12241. [Medline] [CrossRef]
26. **Herrera PL.** Adult insulin- and glucagon-producing cells differentiate from two independent cell lineages. *Development* 2000; **127**: 2317–2322. [Medline]
27. **Kilimnik G, Kim A, Steiner DF, Friedman TC, Hara M.** Intraislet production of GLP-1 by activation of prohormone convertase 1/3 in pancreatic α-cells in mouse models of ß-cell regeneration. *Islets* 2010; **2**: 149–155. [Medline] [CrossRef]
28. **Thorel F, Népote V, Avril I, Kohno K, Desgraz R, Chera S, Herrera PL.** Conversion of adult pancreatic alpha-cells to beta-cells after extreme beta-cell loss. *Nature* 2010; **464**: 1149–1154. [Medline] [CrossRef]
29. **Chung C-H, Levine F.** Adult pancreatic alpha-cells: a new source of cells for beta-cell regeneration. *Rev Diabet Stud* 2010; **7**: 124–131. [Medline] [CrossRef]
30. **Gianani R.** Beta cell regeneration in human pancreas. *Semin Immunopathol* 2011; **33**: 23–27. [Medline] [CrossRef]
31. **Wang Y, Lanzoni G, Carpino G, Cui CB, Dominguez-Bendala J, Wauthier E, Cardinale V, Oikawa T, Pileggi A, Gerber D, Furth ME, Alvaro D, Gaudio E, Inverardi L, Reid LM.** Biliary tree stem cells, precursors to pancreatic committed progenitors: evidence for possible life-long pancreatic organogenesis. *Stem Cells* 2013; **31**: 1966–1979. [Medline] [CrossRef]
32. **Holland AM, Micallef SJ, Li X, Elefanty AG, Stanley EG.** A mouse carrying the green fluorescent protein gene targeted to the Pdx1 locus facilitates the study of pancreas development and function. *Genesis* 2006; **44**: 304–307. [Medline] [CrossRef]
33. **Hara M, Wang X, Kawamura T, Bindokas VP, Dizon RF, Alcoser SY, Magnuson MA, Bell GI.** Transgenic mice with green fluorescent protein-labeled pancreatic beta -cells. *Am J Physiol Endocrinol Metab* 2003; **284**: E177–E183. [Medline]
34. **Elliott RB, Escobar L, Tan PLJ, Muzina M, Zwain S, Buchanan C.** Live encapsulated porcine islets from a type 1 diabetic patient 9.5 yr after xenotransplantation. *Xenotransplantation* 2007; **14**: 157–161. [Medline] [CrossRef]
35. **Orive G, Hernández RM, Gascón AR, Igartua M, Pedraz JL.** Encapsulated cell technology: from research to market. *Trends Biotechnol* 2002; **20**: 382–387. [Medline] [CrossRef]
36. **Watanabe M, Kurome M, Matsunari H, Nakano K, Umeyema K, Shiota A, Nakauchi H, Nagashima H.** The creation of transgenic pigs expressing human proteins using BAC-derived, full-length genes and intracytoplasmic sperm injection-mediated gene transfer. *Transgenic Res* 2012; **21**: 605–618. [Medline] [CrossRef]
37. **Matsunari H, Nagashima H, Watanabe M, Umeyama K, Nakano K, Nagaya M, Kobayashi T, Yamaguchi T, Sumazaki R, Herzenberg LA, Nakauchi H.** Blastocyst complementation generates exogenic pancreas in vivo in apancreatic cloned pigs. *Proc Natl Acad Sci USA* 2013; **110**: 4557–4562. [Medline] [CrossRef]
38. **Umeyama K, Saito H, Kurome M, Matsunari H, Watanabe M, Nakauchi H, Nagashima H.** Characterization of the ICSI-mediated gene transfer method in the production of transgenic pigs. *Mol Reprod Dev* 2012; **79**: 218–228. [Medline] [CrossRef]
39. **Clark AJ, Bissinger P, Bullock DW, Damak S, Wallace R, Whitelaw CBA, Yull F.** Chromosomal position effects and the modulation of transgene expression. *Reprod Fertil Dev* 1994; **6**: 589–598. [Medline] [CrossRef]
40. **Kong Q, Wu M, Huan Y, Zhang L, Liu H, Bou G, Luo Y, Mu Y, Liu Z.** Transgene expression is associated with copy number and cytomegalovirus promoter methylation in transgenic pigs. *PLoS ONE* 2009; **4**: e6679. [Medline] [CrossRef]
41. **Hirabayashi M, Kato M, Ishikawa A, Kaneko R, Yagi T, Hochi S.** Factors affecting production of transgenic rats by ICSI-mediated DNA transfer: effects of sonication and freeze-thawing of spermatozoa, rat strains for sperm and oocyte donors, and different constructs of exogenous DNA. *Mol Reprod Dev* 2005; **70**: 422–428. [Medline] [CrossRef]
42. **Li C, Mizutani E, Ono T, Wakayama T.** An efficient method for generating transgenic mice using NaOH-treated spermatozoa. *Biol Reprod* 2010; **82**: 331–340. [Medline] [CrossRef]

# Supplementary Text

*Physiological characteristics of Pdx1-Venus Tg pigs*

G1 offspring were obtained by breeding the founder Tg pigs with wild-type pigs. The weights of G1 Tg (one female and one male) offspring and a non-Tg (one male) littermate were assessed until the pigs were three months old. The postweaning blood glucose levels of these pigs were measured weekly until the same age. Blood samples collected from the ear vein were analyzed using a human blood glucose meter (Glucocard G+ meter, GT-1820; Arkray, Inc., Kyoto, Japan). At five months old, the fasting and postprandial blood insulin levels of the animals were measured.

Various aspects of blood biochemical parameters were analyzed in three G1 pigs aged between 5 and 15 months of age to determine whether the *Pdx1-Venus* Tg pigs had a normal physiology before and after sexual maturity. As a control, female and male non-Tg pigs, aged between 7 and 8 months of age, from the same litter as the Tg pigs were used. Blood urea nitrogen (BUN), glucose (GLU), creatinine (CRE), total protein (TP), total cholesterol (TCHO), triglyceride (TG), aspartate aminotransferase (AST), alanine aminotransferase (ALT), sodium (Na), potassium (K), and chloride (Cl) were measured using an auto analyzer (DRI-CHEM, FDC-700, Fujifilm, Tokyo, Japan). Insulin concentrations were measured using ELISA (Pig Insulin ELISA KIT (TMB), AKRIN-013T; Shibayagi, Gunma, Japan), and the concentrations of 1,5-anhydroglucitol (1,5-AG) were determined using the standard enzymatic method (SRL, Tokyo, Japan).

Suppl. Fig. 3 shows the physiological features of the Tg pigs and their non-Tg siblings. The G1 Tg piglets grew at the same rate as their non-Tg siblings (Suppl. Fig. 3A).

The non-fasting blood glucose levels of the Tg pigs, which were monitored consecutively after weaning until the pigs were 3 months old, were within the normal physiological range for blood glucose for pigs (Suppl. Fig. 3B). With regard to postprandial blood glucose and insulin levels, the Tg pigs showed similar reactions to those of non-Tg pigs (Suppl. Fig. 3C, D), indicating that the pancreatic functions of *Pdx1-Venus* Tg pigs were normal.

All 13 blood biochemical parameters measured were found to be within the normal ranges in the Tg pigs and their non-Tg control siblings (Suppl. Table 1). Blood 1,5-anhydroglucitol (1,5-AG) levels, indicators of glycemic control during the previous days, were also within the normal ranges in the Tg pigs.

# モーニングセミナー

## レックリングハウゼン病に伴う脊柱変形に対する治療と問題点

○松本　守雄
慶應義塾大学整形外科

脊柱変形はレックリングハウゼン病患者の10-60%に生じるとされており、看過できない問題である。本症による脊柱変形は椎体破壊を伴い急速に進行するdystrophic typeと緩徐に進行するnon-dystrophic typeに大別される。Dystrophic typeでは体幹変形、痛み、肺機能低下、脊髄麻痺など様々な問題を生じることから、変形が著明に進行する前に手術的治療を必要とする場合が多い。手術は骨の脆弱性や腫瘍による骨の浸食によるインプラント設置困難などのため、他の原因による脊柱変形と比較すると遙かに難易度が高い。また、骨癒合不良、インプラント脱転、硬膜損傷など手術に伴う問題点も多い。

本講演では自験例を紹介しながらレックリングハウゼン病による脊柱変形に対する最近の治療法と問題点について概説したい。

共催：ヤンセンファーマ株式会社

ワークショップ

# 次世代シークエンサーを用いたNF1遺伝子診断法の確立

丸岡　亮[1,2]　武内俊樹[3]　清水厚志[4]　鳥居千春[1]　三須久美子[1]　日笠幸一郎[5]　松田文彦[5]
太田有史[6]　谷戸克己[6]　倉持　朗[7]　有馬好美[8]　大塚藤男[9]　吉田雄一[10]　森山啓司[2]
新村眞人[6]　佐谷秀行[8]　小崎健次郎[1]

[1]慶應義塾大学医学部臨床遺伝学センター、[2]東京医科歯科大学大学院医歯学総合研究科顎顔面矯正学分野
[3]慶應義塾大学医学部小児科学教室、[4]岩手医科大学いわて東北メディカル・メガバンク機構
[5]京都大学附属ゲノム医学センター疾患ゲノム疫学分野、6東京慈恵会医科大学皮膚科学講座、[7]埼玉医科大学皮膚科学教室
[8]慶應義塾大学医学部先端医科学研究所遺伝子制御研究部門、[9]筑波大学医学医療系皮膚科
[10]鳥取大学医学部感覚運動医学講座皮膚病態学分野

**要旨**　神経線維腫症1型の原因遺伝子である*NF1*はヒトゲノム中で最も大きい遺伝子の一つであるうえに変異の好発部位が存在しないため、遺伝子診断を行う際全翻訳領域の検索が必要であり本邦ではほとんど行われていない。近年次世代シークエンサーが登場、臨床応用が進められており、我々は先天異常症候群原因遺伝子109を網羅した遺伝子解析パネルを開発、運用を行っている。今回次世代シークエンサーを用い米国国立衛生研究所の臨床基準を満たした神経線維腫症1型患者203例の遺伝子解析を実施した。次世代シークエンサーの解析により203例中159例で病的意義のある変異を検出した。203例の解析の成績により神経線維腫症1型の遺伝子診断に臨床応用が可能であると考えられた。

**Clinical molecular diagnostics of neurofibromatosis type 1 using next-generation sequencer**

Ryo MARUOKA[1,2], Toshiki TAKENOUCHI[3], Atsushi SHIMIZU[4], Chiharu TORII[1], Kumiko MISU[1], Koichiro HIGASA[5], Fumihiko MATSUDA[5], Arihito OTA[6], Katsumi TANITO[6], Akira KURAMOCHI[7], Yoshimi ARIMA[8], Fujio OTSUKA[9], Yuichi YOSHIDA[10], Keiji MORIYAMA[2], Michihito NIIMURA[6], Hideyuki SAYA[8], Kenjiro KOSAKI[1]

[1] *Center for Medical Genetics, Keio University School of Medicine, Tokyo, Japan*
[2] *Section of Maxillofacial Orthognathics, Department of Maxillofacial Reconstruction and Function, Division of Maxillofacial / Neck Reconstruction, Graduate School, Tokyo Medical and Dental University, Tokyo, Japan*
[3] *Department of Pediatrics, Keio University School of Medicine, Tokyo, Japan*
[4] *Iwate Tohoku Medical Megabank Organization, Iwate Medical University, Iwate, Japan*
[5] *Center for Genomic Medicine, Kyoto University Graduate School of Medicine, Kyoto, Japan*
[6] *Department of Dermatology, Jikei University School of Medicine, Tokyo, Japan*
[7] *Department of Dermatology, Saitama Medical University, Saitama, Japan*
[8] *Division of Gene Regulation, Institute for Advanced Medical Research, Keio University School of Medicine, Tokyo, Japan*
[9] *Department of Dermatology, Institute of Clinical Medicine, University of Tsukuba, Tsukuba, Japan*
[10] *Division of Dermatology, Department of Medicine of Sensory and Motor Organs, Faculty of Medicine, Tottori University, Yonago, Japan*

The *NF1* gene, the causative gene for neurofibromatosis type 1, is one of the largest genes in the human genome, making it a relatively difficult for molecular diagnosis. The recent advent of next-generation sequencing technology has enabled many genes, regardless of the size of the genes, to be analyzed at once. For the clinical diagnostic purpose, we developed customly-designed mutation analysis panel using enrichment system covering 109 genes which are causative genes for classic multiple congenital anomalies syndromes. Here we conducted the next-generation sequencing protocol to identify mutations for 203 patients with neurofibromatosis type 1 who met the NIH clinical diagnostic criteria. The next-generation sequencing protocol led to the identification of pathological mutations in 159 of the 203 patients. The results showed the clinical utility of this next-generation sequencing method in the diagnosis of neurofibromatosis type 1.

**Key words :** *NF1*, molecular diagnosis, next-generation sequencing

## 緒　言

神経線維腫症1型は、カフェオレ斑、皮膚の神経線維腫、腋下および鼠径部の色素斑、虹彩過誤腫などを主症状とする常染色体優性の遺伝形式をとる疾患である。原因遺伝子として17q11.2に存在する*NF1*遺伝子が同定されている。*NF1*は約280kbp、58エクソン、2818アミノ酸で構成され、ヒトゲノム中で最も大きい遺伝子の一つである。*NF1*はその大きさ及び変異の好発部位が存在しないため全翻訳領域の解析が必要になることから臨床検査としての遺伝子検査は本邦ではほとんど行われていない。

近年、次世代シークエンサーが登場、臨床応用がすすめられており、我々は*NF1*を含む先天異常症候群の原因とされている遺伝子109を網羅した次世代シークエンサー解析パネルを開発、運用を行っている。今回我々は次世代シークエンサー解析パネルを用い神経線維腫症1型患者の遺伝子解析を行ったので報告する。

## 方　法

対象は米国国立衛生研究所の臨床診断基準[1]を満たした203例とした。各施設にてインフォームドコンセントを得た後、末梢血を採取、慶應義塾大学医学部臨床遺伝学センターにて解析を行った。

通法に従いゲノムDNAを採取、Life technologies社Qubitにて定量を行ったのち、DNA 3μgをCovaris社超音波DNA断片化装置を用い約150bpに細断し解析に用いた。標的遺伝子領域の濃縮はAgilent Technologies　社SureSelect Target Enrichment systemを用いin-solution hybridizationにて行った。SureSelectの設計はAgilent TechnologieseArrayシステムを用いた。濃縮を行ったDNAはPaired-end read sequencing system（Illumina社MiSeq system）にてシークエンスを行った。

得られたリードはFASTQファイルとして出力し、Burrows-Wheeler Alignment tool、The Genome Analysis Toolkit package、snpEffなどのオープンソースプログラムを用い解析を行った。またdbSNP version 135、the 1000 Genomes Projectおよび正常日本人1208人の多型データーベース[2]それぞれに記載されている多型を除外した。またRas pathway上の遺伝子（*PTPN11, KRAS, SOS1, RAF1, SHOC2, HRAS, BRAF, MAPK1, MAP2K1, MAP2K2, MAPK3, SPRED1,RASA1*）の多型に関してはその病的意義の検証を行い、それ以外の遺伝子は偶発的な所見による潜在的な倫理的問題を避けるため確認を行わなかった。

はじめに検査を行った86例では、次世代シークエンサー解析によりナンセンス変異、フレームシフト変異、またスプライスドナーサイトおよびアクセ

プターサイトに変異が認められた場合、またミスセンス変異で、過去に文献にて病的と報告のあった変異が検出された場合、直接シークエンス法により変異の確認を行った。また以上の変異が認められない場合は、*NF1* 全エクソンを直接シークエンス法により確認した。直接シークエンス法は通法に従い、プライマーを作成、解析は Life Technologies 社 ABI BigDye version1.1 Terminator Cycle Kit を使用し Life Technologies 社 ABI Prism 3500 Capillary Array Sequencer にてシークエンスを行った。また *NF1* 遺伝子の複数ないし遺伝子全体の重複・欠失の検索を行うため、multiplex ligation-dependent probe amplification method（MLPA）法を行った。解析は MRC-Holland 社 SALSA P081/082-B2 NF1 MLPA assay kit を用いプロトコールに従い解析を行った。文献報告のないミスセンス変異はその病的意義に関して、SIFT [3], Polyphen2 [4], LRT [5], Mutation Taster [6], PhyloP [7] の5つのバイオインフォマティクスアルゴリズムにより評価を行った。5つのアルゴリズムのうち4つ以上で病的と推定されたもの（SIFT により 'damaging', Polyphen2 により 'probably damaging', LRT により 'deleterious', Mutation Taster により 'disease causing', PhyloP により 'conserved'）は、病的な変異の可能性が高いと解釈した（図1）。

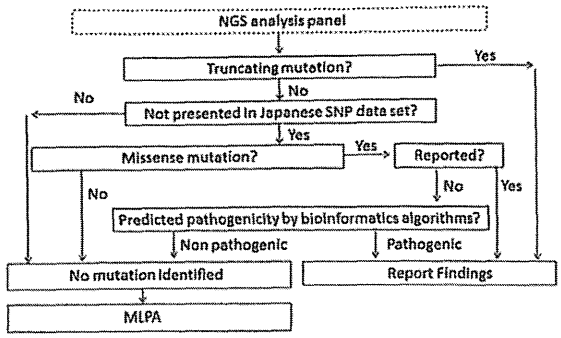


図1　変異解析の流れ

## 結　果

はじめに検査を行った86例では次世代シークエンサー解析により70例で病的意義のある変異を検出することができた。すべての変異はヘテロ接合性であり、58例で truncating mutation を認めた。12例でミスセンス変異を認め、そのうち9例で過去に文献にて機能解析及び家族歴から病的変異との報告があった。残り3例はバイオインフォマティクスアルゴリズムにて推定を行い、c.2183T>G (p.Val728Gly) の変異は5つのアルゴリズムにて病的と判定され、c.2540T>G (p.Leu847Arg) 及び c.6818A>T (p.Lys2273Met) は5つのアルゴリズムのうち4つで病的と判定された。上記3例に加え、次世代シークエンサー解析にて病的変異を認めなかった16例は MLPA 法にて欠失の判定を行い10例で欠失（*NF1* 全体の欠失5例、複数エクソンの欠失2例、1エクソンの欠失3例）を認めた。

残りの117例は次世代シークエンサーによる解析のみを行い、前述の86例と合わせ203例中159例で病的意義のある変異を認めた（図2）。

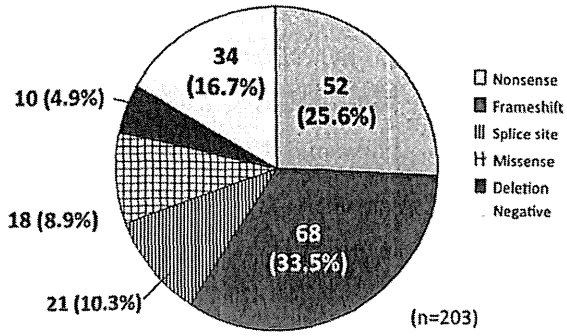


図2　変異解析の結果

## 考　察

本研究ではじめに解析を行った86例の結果から、in-solution hybridization を用いた次世代シークエンサー解析により標準的な方法である直接シークエンス法と同等の検出率で遺伝子解析を行うことができることが示された。この結果は次世代シークエンサーを用いた遺伝子解析が *NF1* の遺伝子診断に臨床応用が可能であると考えられた。

今回の解析の病的変異検出率は203例中159例、78.3%であった。この値は必ずしも高い検出率とは

言えない。ここで先に解析を行った86例で前述の通り次世代シークエンサーでは原理的に検出することのできない複数エクソンにわたる重複・欠失の検索をMLPA法にて検査を行い、病的変異が認められなかった16例中10例で欠失を認めたことに着目すると、117例（全203例-86例）中で変異を認めない28例においても相当数が大きな欠失を有している可能性が高いと考えられる。MLPA法による解析の結果によって最終的な変異陽性率を算出する必要があると考えられる。

このMLPA法でのみ検出可能である複数エクソンにわたる欠失に関して、次世代シークエンサーで解析が可能となるプログラムが報告されはじめており、近い将来重複・欠失検出が可能となると思われ、さらなる検討が必要であると考えられた。

## 結　語

203例の神経線維腫症1型患者の遺伝子解析の結果よりin-solution hybridizationを用いた次世代シークエンサー解析系は臨床応用が可能であると考えられた。

## 文　献


1) Neurofibromatosis Conference statement: National Institutes of Health Consensus Development Conference. Arch Neurol 45 : 575 - 8 , 1988 .
2) Japanese genetic variation consortium. [http://www.genome.med.kyoto-u.ac.jp/SnpDB]
3) Kumar P, Henikoff S, Ng PC: Predicting the effects of coding non-synonymous variants on protein function using the SIFT algorithm. Nat Protoc 4 : 1073 - 81 , 2009 .
4) Adzhubei IA, Schmidt S, Peshkin L et al.: A method and server for predicting damaging missense mutations. Nat Methods 7 : 248 - 9 , 2010 .
5) Chun S, Fay JC: Identification of deleterious mutations within three human genomes. Genome Res 19 : 1553 - 61 , 2009 .
6) Schwarz JM, Rödelsperger C, Schuelke M et al.: MutationTaster evaluates disease-causing potential of sequence alterations. Nat Methods 7 : 575 - 6 , 2010 .
7) Siepel A, Pollard KS, Haussler D: New methods for detecting lineage-specific selection. Proceedings of the 10 th International Conference on Research in Computational. Molecular Biology 3909 : 190 - 205 , 2009 .


## 謝　辞

本論文は、平成22年9月28日にご逝去された杉江史子様のご遺志により、ご実弟であられる杉江悠司様を介して日本レックリングハウゼン病学会に寄付された2,500万円の浄財によって為された研究の一部を取りまとめたものである。既に200例を超える遺伝子解析をこの資金によって実施しており、今後その成果について随時報告を行う予定である。杉江様の多大なるご貢献に対し、日本レックリングハウゼン病学会一同、深く感謝の意を表するものである。